

**Reproducing Human Motion using Force Intervention
by Humanoid Robot: Application to Evaluation of
Wearable Assistive Device**

March 2020

Ito Takahiro

**Reproducing Human Motion using Force Intervention
by Humanoid Robot: Application to Evaluation of
Wearable Assistive Device**

**Graduate School of Systems and Information Engineering
University of Tsukuba**

March 2020

Ito Takahiro

Abstract

Humanoid robots have a big potential to be human co-workers in industrial fields or personal assistants in daily life. Besides being workers or assistants, they can be used as human body simulators instead of human subjects in order to understand human itself. For this purpose, this thesis addresses the human motion reproduction with a humanoid robot. Our motion reproduction method includes not only the geometric movement but also the physical interaction between human and the environment or the devices that the human uses. The main objective of this research is the human movement when a human utilizes the device and evaluate its assistive effects by using humanoid robot because many wearable assistive devices are developed for reducing a physical burden on human body, therefore, social impact of their evaluation is big. For determining the interaction model when human utilize the device, human motion measurements of muscular activity are conducted. Analysis of the measured muscle activity revealed the human strategy of the actual usage of assistive devices. By considering the strategy, the humanoid controller that reproduces the human motion in similar manner with human is proposed. The contact estimation method for humanoid robots is also proposed to understand the interaction situation between the robot and the device. Finally, proposed components are combined into a control framework for realizing the interaction-based motion reproduction on humanoid robot. To the application for evaluating the device, the proposed control framework is applied to the evaluation of the device. The effectiveness of our application is validated by experimentally assessing an assistive device Muscle Suit actuated by pneumatic artificial muscles with humanoid robot HRP-4.

Acknowledgements

I would like to express my sincere gratitude to my supervisor Professor Eiichi Yoshida for his continuous support and encouragement throughout this endeavour. He always kindly guided me to achieve all results of this thesis even when he was very busy.

Also, I would like to express special appreciation to Dr. Ko Ayusawa. Together with my supervisor, he checked every result that I obtained, reviewing every writing and presentations. Every time I got stuck with my research he was there to help me.

I would like to thank Professor Abderrahmane Kheddar for giving me the opportunity to continue my research at LIRMM in France.

I would like to thank to my sub-supervisors Professor Hiromi Mochiyama and Associate Professor Hisashi Date for giving me helpful advices and supporting me in the University of Tsukuba. Also, I would like to thank Professor Humio Kanehiro as my jury. They spent a lot of time checking this thesis in detail.

I would like to thank Professor Hiroshi Kobayashi for providing me the wearable assistive device Muscle Suit and many advice related to the device evaluation. Without his help, all the results related to the device evaluation could not be achieved.

Special thanks to all members of CNRS-AIST Joint Robotics laboratory. To Yumeko Imamura, Yusuke Yoshiyasu, Adrien Escande, Pierre Gergondet, Naoko Sakai and Ryusuke Sagawa, They always gave me timely assistance throughout my research life in the laboratory. To Antonio, Ashesh, Kai, Sylvain, Vincent, Kevin, Jihong, Arnoud and all my colleagues, I have had the support and encouragement of them throughout both my research life and daily life.

Finally, I would like to thank my family and my friends for supporting me throughout my daily life.

Contents

| | |
|--|-------------|
| Abstract | ii |
| Acknowledgements | iii |
| List of Figures | viii |
| List of Tables | xiii |
| 1 Introduction | 1 |
| 1.1 Research Background | 3 |
| 1.1.1 Humanoid Robot as Human Body Simulator | 4 |
| 1.1.2 Wearable Assistive Devices and their Evaluation | 5 |
| 1.2 Goal of Thesis | 6 |
| 1.3 Thesis structure | 7 |
| 2 Human Motion Analysis and Extraction of Strategy using Force Intervention | 9 |
| 2.1 Introduction | 9 |
| 2.2 Human Muscle Activity Analysis with Wearable Assistive Device . . | 10 |
| 2.2.1 Problem Statement of Human Motion Analysis when Using Devices | 10 |
| 2.2.2 EMG Measurements and Human Motion Analysis Wearing the Device | 11 |
| 2.3 Experimental Environment of Human Motion Measurement | 15 |

iv

| | | |
|----------|---|-----------|
| 2.3.1 | Assistive Device for Lower Back: Muscle Suit | 15 |
| 2.3.2 | Measurement Setup for Human Motion | 15 |
| 2.4 | Muscle Activity analysis with Muscle Suit | 16 |
| 2.5 | Conclusion | 18 |
| 3 | Contact Estimator on Humanoid Robots for Observing Force In- | |
| | tervention | 20 |
| 3.1 | Contact Estimation on Humanoid Robot | 21 |
| 3.1.1 | Contact Detection and Identification | 21 |
| 3.1.2 | Contact Link and Point Estimation | 22 |
| 3.2 | Experimental Validation of Contact Estimation | 24 |
| 3.2.1 | Contact Estimation in Simulation | 25 |
| 3.2.2 | Contact Estimation on the Real Humanoid Robot and Prac- | |
| | tical Discussions | 27 |
| 3.3 | Conclusions | 32 |
| 4 | Human Motion Reproduction of Assistive Device Usage on Hu- | |
| | manoid Robot | 34 |
| 4.1 | Introduction | 34 |
| 4.2 | Torque-based Human-motion Tracking Control | 35 |
| 4.2.1 | Assumptions of Human Behavior with Assistive Devices . . | 35 |
| 4.2.2 | Human Motion Retargeting for Humanoid | 36 |
| 4.2.3 | Path Tracking Control with Joint Torque feedback | 37 |
| 4.3 | Experiments | 39 |
| 4.3.1 | Experiment Setup | 39 |
| 4.3.2 | Experiment of Proposed Control Scheme | 40 |
| 4.4 | Conclusion and Discussion | 43 |
| 5 | Humanoid Controller for Motion Reproduction including Force | |
| | Intervention | 46 |
| 5.1 | Introduction | 46 |

| | | |
|----------|--|-----------|
| 5.2 | Vector Field based Tracking Controller | 47 |
| 5.2.1 | External Torque Observer | 49 |
| 5.2.2 | Tracking Controller based on External Torque | 50 |
| 5.3 | Experiments on Humanoid | 53 |
| 5.3.1 | Experimental Setup | 53 |
| 5.3.2 | Experimental Validation of Proposed Controller | 55 |
| 5.4 | Conclusion and Discussion | 57 |
| 6 | Assistive Device Evaluation with Humanoid Robot | 59 |
| 6.1 | Experimental Setup | 59 |
| 6.2 | Evaluation Framework for Wearable Assistive Device | 60 |
| 6.3 | Conclusion and Discussion | 66 |
| 7 | Conclusion | 70 |
| | Bibliography | 74 |
| | List of Publications | 83 |

List of Figures

| | | |
|-----|--|----|
| 1.1 | Humanoid Robots | 4 |
| 2.1 | Example of upper-limb model. | 12 |
| 2.2 | Simplified spinal muscular skeletal model. | 13 |
| 2.3 | Overview of human motion experiment and muscle activity analysis. | 14 |
| 2.4 | The specific structure of Muscle Suit | 16 |
| 2.5 | Humanoid robot HRP-4 and Muscle Suit. The device is attached on shoulders, waist, and thighs in exactly the same way as a human does. | 17 |
| 2.6 | Snapshot of experimental set up | 18 |
| 2.7 | Estimated torque with 5 kg weight; the blue line shows τ_{dyn} estimated by inverse dynamics computation (i.d.), red line shows the τ_{Joint} estimated using Equation (2.5) with IEMG signals, and green line shows the waist joint angle. | 18 |
| 2.8 | Estimated torque with 10 kg weight; the blue line shows τ_{dyn} estimated by inverse dynamics computation (i.d.), red line shows the τ_{Joint} estimated using Equation (2.5) with IEMG signals, and green line shows the waist joint angle. | 19 |

| | | |
|-----|--|----|
| 3.1 | Contact link searching algorithm. The contact force is applied to link l_{i+2} the contact force generates the error torque τ_{i+2} at self-joint and every predecessor joint until base link but no error torque is generated at the links in another branches like link l_j , l_m or l_n . Tracing the link containing the error torque, the contact link can be found. | 23 |
| 3.2 | Applying a single force to left and right hands in simulation. The force applied to left elbow link is fixed and the direction of the force applied to right arm is moving down. | 26 |
| 3.3 | Result of contact link detection, force strength identification and contact point estimation in simulation. Upper part indicates force strength of contact force and lower part indicates the contact link index (No. 21 is right elbow link, No. 30 is left elbow link). | 27 |
| 3.4 | Reconstructing a line of action of contact forces and computing the intersections between a line and the robot body mesh. Right side figure shows the result of the left elbow link and the left side shows that of the right one. The detected contact links are highlighted in red. | 28 |
| 3.5 | Applying a single force to right and left arms in HRP-4. The force was applied to right elbow link (a), right shoulder link (b) then, left elbow link (c), left shoulder link (d) by fixed direction. | 30 |
| 3.6 | Result of contact link detection, force strength identification and contact point estimation in HRP-4. Left y -axis indicates the force strength of contact force and right y -axis indicates the contact link index (No. 21-23 is right shoulder link, No. 24 is right elbow link, No. 30-32 is left shoulder link and No. 33 is left elbow link). | 31 |
| 3.7 | Reconstructing a line of action of contact forces and computing the intersections between a line and the joined body mesh. The joined body surface of left shoulder link and elbow link are shown in red. Right side figure shows the result of left link and left side shows that of right one. | 32 |

| | | |
|-----|---|----|
| 4.1 | Relationship between joint angle trajectory and a trajectory parameter x (ex. 3DOFs). Each value of $\theta_i(i = 1, 2, 3)$ is derived from the one-by-one mapping function $\boldsymbol{\theta}(\mathbf{x}): [\theta_1 \ \theta_2 \ \theta_3]^t = \boldsymbol{\theta}(x), x_0 \leq x \leq x_1$ | 37 |
| 4.2 | Humanoid HRP-4 (softcover) | 40 |
| 4.3 | Waist joint torque and velocity of parameter x ($0 \leq x \leq 1$). The robot motion starts at 4 [sec] when the waist joint torque becomes zero. The motion is maintained for 7 s and ends at around 11 s. | 42 |
| 4.4 | Original human motion and retargeted humanoid motion. In human motion measurement, a human subject used the exhalation switch to activate the assistive device (Muscle Suit), and then lifted a 5-kg weight. The device provided the supportive force while switch is turned on. In the humanoid robot experiment, two 2-kg weights were attached to each wrist joint, and the device was activated by a switch controlled by an experiment operator. The robot started the lifting motion when the device was activated and provided enough supportive torque. | 44 |
| 5.1 | Overview of our controller | 49 |
| 5.2 | Relationship between the desired state $(x, f_{(x)})$ in the interaction model and a current robot state $(x, \hat{\tau}_{ast})$ with the vector field. The solid line is the target trajectory $f_{(x)}^{trg}$ generated by the motion retargeting method and the arrows denote the gradient vectors at each point in the space. | 51 |
| 5.3 | Defining the vector at the point $C(x, \hat{\tau}_{ast})$. $x, \hat{\tau}_{ast}$ are current state, $f_{(x[i])}^{trg}$ is the closest point of trajectory from C , $i = 1, 2, \dots, n$. | 53 |
| 5.4 | Result of human motion reproduction by the proposed controller. When the assistive device is activated (starts supporting), the robot starts lift-up motion ((a)-(c)). After achieving an upright posture (d), the robot keeps the posture until the device is deactivated. Finally, the robot put the weight down while the supportive effect decreases ((e)-(g)). | 54 |

| | | |
|-----|--|----|
| 5.5 | Result of assistive torque observer (upper row) and tracking controller (lower row). | 56 |
| 6.1 | Procedure of the assistive torque extraction; step 1) measuring the joint torques with the device by using the proposed controller; step 2) measuring the joint torques without the device by playing-back the motion recorded in step 1; step 3) comparing the joint torques measured with device and without device. | 61 |
| 6.2 | Torque comparison of the lift-up 4kg weight motion with the device and without device. The motion starts around 6 s when the joint torque changes. The motion continued for 15 s until it ended around 21 s. The motion is divided by 3 periods; first period (6-13 s) is corresponding to motion depicted in (a) to (c) in Figure 5.4, second period (13-18 s) is corresponding to motion depicted in (d) in Figure 5.4, last period (18-21 s) is corresponding to motion depicted in (e) to (g) in Figure 5.4. | 63 |
| 6.3 | Torque comparison of the lift-up 6kg weight motion with the device and without device. The motion starts around 4 s when the joint torque start changes. The motion continued for 17 s until it ended around 22 s. | 63 |
| 6.4 | Hip joint torque comparison of the lift-up 4kg weight motion with the device and without device. | 64 |
| 6.5 | Knee joint torque comparison of the lift-up 4kg weight motion with the device and without device. | 64 |
| 6.6 | Result of the assistive torque extraction. The blue line denotes the assistive torque with 4-kg weight and the red one denotes that with 6-kg weight | 65 |
| 6.7 | All joint torque comparison of the lift-up 4kg weight motion with the device and without device. In all results, the blue solid line shows the torque when using the device and the red line indicates that without the device. | 67 |

6.8 All joint torque comparison of the lift-up 6kg weight motion with the device and without device. In all results, the blue solid line shows the torque when using the device and the red line indicates that without the device. 68

List of Tables

| | | |
|-----|---|----|
| 6.1 | Comparison of mass properties between human and HRP-4 | 60 |
| 6.2 | Experimental condition in step 1) and 2) | 62 |

Chapter 1

Introduction

Humans have advanced motor functions and can achieve complex movements by interacting with the environment. The mechanism of human structure and its control system attract the interest of researchers in the field of robotics. Humanoid robots are human-like shaped robots, developed for various purpose such as human assistants, co-workers and rescue workers in disaster area. For this purpose, several research fields have been developed; bipedal locomotion, dual-arm manipulation and human-robot interactive task. Humanoid robotics can contribute to the development of the robot that can be used in a real environment designed for humans. The major advantage of the humanoid robot is that the robot can achieve the task in same manner to that of humans: the robot can use tools designed for humans, and move around in the human environment. In addition, they can be used as the human body simulator to get the deeper understanding of information about humans. By using these advantages, recent researches introduced the devices to support human motion: for example, applying the control theory of the bipedal walking, the robotic device for walking support was developed. These researches for the human-centered design of the device are attracting more and more, and expected as the solution for social problem such as aged society by using the robotics technology.

In this thesis, we use the humanoid robots as human body simulator to evaluate the human-centered robotic devices for physical body support. Therefore, we

focus on the human motion when using the robotic devices and realize the motion reproduction by using the humanoid robot.

The motivation of this study comes from the need to analyze the internal forces during the human motion using the *force intervention*, that is, the external force exertion by the physical interaction with others in collaboration tasks, or the wearable robotic devices. Analyzing the motion when using the force intervention, we can study how humans use the benefit of the external force, and also develop the robot controller that can adapt the external force. The motion using the force intervention can be regarded as a part of physical interaction. In most human motion in physical interaction, humans apply the forces to environment to get the reaction forces to achieve the motion such as standing up or walking. On the other hands, the force intervention is achieved by the external forces from environment and defined as follows in this study:

Definition 1 (force intervention). *In this thesis, force intervention is defined as the process of applying external forces that contribute to achieve tasks.*

The difficulty of the analysis is due to the limitation in human subject experiments such that force measurement on human body is not available. Alternatively, the dynamic simulation using digital human models can provide the human body analysis. These methods are emerging in the field of computer graphics to generate the 3D character motions, and human-centered design (ergonomics) to create the better tools for human bodies. However, the simulation relies on the provided models, therefore, the accuracy of the models, especially models for reconstructing the physical interaction between human body and the devices, is major issue. Using the humanoid robot as human body simulator is the solution to provide the estimation of the human internal loads in same physical environment as that human subjects do.

To use the humanoid robot as human body simulator, human motion reproduction with the robot is required. The motion reproduction has two aspects; (i) the geometrical motion reproduction that the robot reproduces the same movement trajectory as human movement, and (ii) the physical interaction reconstruction

that the robot interacts with the environment in same manner to that human does. The geometrical reproduction (i) has been achieved in several study which is detailed in next section. Most studies use motion capture system to record the human motion and convert the motion trajectory of recorded trajectory to humanoid motion trajectory. Although the methods take into account the balancing, the dynamic behavior during physical interaction is not considered. Therefore (ii) is important to understand the human behavioral intention during the motion and imitate the motion. Since we focus on the human motion when using the robotic devices in this study, the interaction between the body and the device can be described as force intervention; the external force exertion applied by the device. In this thesis, we first introduce the method to observe the force intervention on human subject experiment, and extract the human behavioral intention when using the force intervention. Then, by considering the human behavioral intention, the control framework of the humanoid robot to reproduce human motion is developed. Finally, the device evaluation is achieved by using the humanoid robot as human body simulator.

In the next section, the general background of humanoid robots and its use as human body simulator is to be addressed.

1.1 Research Background

Humanoid robots are designed to have a similar structure to that of humans so that they can move like humans. Currently, these robots are widely developed [1, 2, 3, 4, 5] and expected to human co-workers in industrials fields or dangerous areas like disaster sites and space.

One of the most representative humanoid robot is ASIMO (Figure 1.1 (A)) [6, 7], developed at HONDA and first appeared in 2000. The latest version of ASIMO can recognize the surrounding environment by visual and auditory sensors , and achieve various motion such as walking, running and hoping while balancing. Another representative one is iCub (Figure 1.1 (B)) [8] developed at the Italian institute of technology. Its hands have 9 actuated degrees of freedom (dof) so as



(A) ASIMO [6] (B) iCub [2] (C) HRP-2 Kai [11] (D) ATLAS [10]

Figure 1.1: Humanoid Robots

to achieve dexterous manipulation and tactile sensors integrated in the finger tips [9]. As an example of a human-sized humanoid robot, ATLAS (Figure 1.1 (C)) from Boston Dynamics [10] is 1.5 m height and 80 kg weight humanoid robot, that has hydraulic joints and can achieve the complex dynamic movement such as hopping and doing back-flips. HRP-2Kai [11] (Figure 1.1 (D)) developed at national institute of advanced industrial science and technology (AIST) in Japan is also a human-sized one, which is improvement version of HRP-2 [12]. This robot is 1.5 m height, 60 kg weight and designed for inspection and disaster response in social infrastructures.

1.1.1 Humanoid Robot as Human Body Simulator

Humanoid robots are also used extensively for mechanical simulation of the human body. By controlling a humanoid robot in actual environment, we can obtain the knowledge about a human body and motion. A similar application is traditionally found in automotive crash-testing experiments, in which a humanoid dummy is used to obtain quantitative data such as the impact of a collision on the dummy.

Some studies have used humanoid robots instead of human subjects to evaluate products intended for human use. Takanishi et al. developed the WABIAN-2 humanoid robot [13] for use as a dynamic simulator to test a walking support device during locomotion [14]. Nelson et al. developed the PETMAN robot [15] to reproduce a large range of human motion for testing chemical-protective clothing.

Using humanoid robots as human simulators gives following advantages.

- Robots provide quantitative measurements by internal sensors.
- Robots can reproduce motions with high repeatability throughout the experiment.
- There is no requirement of institutional review board approval unlike experiments with human subjects.

By reproducing the human motion with humanoid robot, Miura et al. and Ayusawa et al. introduced an evaluation framework for wearable assistive devices [16, 17, 18]. The framework was realized by utilizing the key technology of motion retargeting [18], which allows a humanoid robot to reproduce human-like motions. These motion reproduction or imitation method on humanoid robot have been developed in several researches [19, 20, 21]. Mostly, these motion reproduction methods use three-dimensional position of markers on human body measured by motion capturing system and map them to humanoid body, then compute inverse kinematics to obtain the joint angle trajectory. Although these methods can realize geometrical motion reproduction, it cannot be extended to the human motion using force intervention by environment or the devices such the case that human utilizing an active assistive device (also referred to as exoskeleton).

1.1.2 Wearable Assistive Devices and their Evaluation

Recently, the assistive devices have been widely developed. There are several researches about various robotic assistive devices such as the device for walking [22, 23], for monitoring one's health [24], for manipulating heavy objects [25, 26],

for reducing caregiver load or the elderly and patients support [27, 28], and for rehabilitations [29, 30]. These robotic devices, especially the wearable type of assistive devices, are a promising option not only for caregivers but also for any worker who performs heavy load tasks to reduce stress on the lower back.

Definition 2 (Wearable Assistive Device). *Wearable assistive devices are the robotic suit to support the human body by applying the assistive forces from its actuators. They are also referred to as Exoskeletons, lightweight and easy-to-wear tools among them in particular.*

Some commercial products of these devices are already available [31, 32, 33]. The market of these devices is now exploding and thus requires a method to test the different commercial products quantitatively to let the users compare them.

Human motions with the wearable assistive device are the special cases of the motion with a general devices or tools. Most of the assistive devices are designed by considering the human body structure and the movements so that the users can achieve the natural movements when they are using the devices. As a result, a part of the human body is replaced with the device by wearing it, and they can achieve the movement while getting the benefit of the device assists. These human cooperative movements using *force intervention* by the device is one of the difficult situation to reproduce by using the humanoid robot with motion retargeting method. To achieve the human motion reproduction using force intervention, the humanoid robot needs to perform the motion in the similar manner to the physically interactive behavior of humans.

1.2 Goal of Thesis

In this thesis, we define the human motion reproduction using force intervention by an assistive device as the main goal of this thesis for following reasons:

1. using a wearable assistive device is a typical example of human motion including force intervention by a device.

2. motion reproductions on humanoid robot when using the assistive devices allow to evaluate the devices by measuring the supportive force that is difficult to be measured in experiments on human subjects.

Therefore, the human motion reproduction when using these devices and their evaluations have a big social impact such as a standard of the assistive device. In fact, the Japanese Industrial Standards (JIS) committee published the standard for lumbar support wearable assistive devices [34, 35].

To achieve this goal, firstly, human motion experiments are conducted for recording the motion trajectory when using a device. Then we determine the human motion strategy using force intervention by the device by measuring muscular activities. The result of the experiment is used to develop a controller that realizes the humanoid motion in similar manner to humans. Because the interaction between a robot and a device should be considered to estimate the external forces due to force intervention by the device, the contact estimation method for humanoid robot is also introduced to observe the external force applied by the device. Finally, the humanoid control framework for the human motion reproduction including changes of human strategy is proposed.

In this thesis, we also introduce an evaluation framework for active assistive devices by using the proposed controller. The novelty of this research lies in its capacity for quantitative evaluation by closely reproducing the scenarios in which humans use assistive devices with feedback data from the robot's sensors.

1.3 Thesis structure

This thesis is organized as follows. In Chapter 2, the method to observe the force intervention during human subject experiment is to be addressed. Human muscular activity during a motion with force intervention applied by the assistive device is measured to analyze a human motion strategy. Then, the practical contact estimation for humanoid robots is presented in Chapter 3 to allow a robot to observe the force intervention. In Chapter 4, we propose the humanoid controller

that realize motion reproduction with considering human motion strategy. After introducing all related components, the vector field-based human motion reproduction method is presented in Chapter 5. Since the proposed controller can be used for evaluation of assistive devices, the example of device evaluation is shown in Chapter 6. Finally, Chapter 7 concludes the thesis by discussing the feasibility and effectiveness of the proposed method.

Chapter 2

Human Motion Analysis and Extraction of Strategy using Force Intervention

2.1 Introduction

In this chapter, the human motion analysis when using the assistive device is described. We first mention the general technique to analyze the human motion by using the human skeletal model, and its limitations for extending it to our case that human motion using the force intervention by the device. Then, we introduce the method to observe the force intervention, and extract the strategies of the assistive device use.

The human body is often modeled as an articulated multi-body system in a manner similar to the modeling of a humanoid robot [36, 37]. Recently, human skeletal (musculoskeletal) modeling and its dynamic simulation have developed to simulate and estimate the biomechanical causes of movements. OpenSim [38, 39] is open source software system that realize developing models of musculoskeletal structures and creating dynamic simulations of movement. AnyBody [40, 41] is also musculoskeletal modeling and simulation tools developed by AnyBody Technology. These simulations allow to analyze the musculoskeletal system of humans

and estimate the internal force of humans during walking [42], swimming [43] and weight lifting motion [44]. Some studies presented the evaluation or design method of wearable assistive devices [45, 46], however, the methods have following limitations addressed in section 2.2.1.

2.2 Human Muscle Activity Analysis with Wearable Assistive Device

2.2.1 Problem Statement of Human Motion Analysis when Using Devices

Human motion analysis on dynamic simulation is based on human and its surrounding modeling, and inverse dynamics computation, therefore, the method has following problem:

1. The models of human body and its surrounding environment are required. The models involve the mechanical parameters as well as the controller to achieve the motion reproduction on simulation. The computer aided design (CAD) tools can provide the mechanical parameters of the devices, However, most devices are consist of the soft materials to make soft contact between the device and the human body, and they are difficult to be modeled.
2. The physical interaction model between human body and environment is required. To achieve the dynamic analysis, the physical interaction model is also necessary to reproduce the contact situation: which parts of human bodies are in contact (surface contacts or point contacts), how much forces are applied to the body. However, reconstructing the contact situation in simulation is very difficult due to difficulty of measurement of the internal forces in human body.
3. The accuracy of the simulation results depends on the models introduced in 1 and 2.

Moreover, even if the models can be well reconstructed, it is difficult to distinguish the supportive torque from the human joint torque owing to redundancy of the contact forces between the body and the device. For example, in the case of human upper-limb, we can assume the simplified model of upper-limb like shown in Figure 2.1. Introducing the human skeletal model as articulated multi-body, the dynamics of the model can be formulated as Equation (2.1).

$$\boldsymbol{\tau}_{Joint} + \boldsymbol{\tau}_{ext} = \boldsymbol{\tau}_{dyn}(\boldsymbol{\theta}, \dot{\boldsymbol{\theta}}, \ddot{\boldsymbol{\theta}}). \quad (2.1)$$

where $\boldsymbol{\theta}$, $\dot{\boldsymbol{\theta}}$ and $\ddot{\boldsymbol{\theta}}$ are the vectors of generalized coordinates, velocities and accelerations, respectively. $\boldsymbol{\tau}_{joint}$ is vector of joint torques and $\boldsymbol{\tau}_{ext}$ is vector of external torques. In the human motion analysis, $\boldsymbol{\tau}_{dyn}(\boldsymbol{\theta}, \dot{\boldsymbol{\theta}}, \ddot{\boldsymbol{\theta}})$ can be estimated through inverse dynamics computations of a human skeletal model:

$$\boldsymbol{\tau}_{dyn}(\boldsymbol{\theta}, \dot{\boldsymbol{\theta}}, \ddot{\boldsymbol{\theta}}) = \mathbf{M}(\boldsymbol{\theta})\ddot{\boldsymbol{\theta}} + \mathbf{C}(\boldsymbol{\theta}, \dot{\boldsymbol{\theta}}) + \mathbf{G}(\boldsymbol{\theta}) \quad (2.2)$$

where $\mathbf{M}(\boldsymbol{\theta})$ is the inertia matrix, $\mathbf{C}(\boldsymbol{\theta}, \dot{\boldsymbol{\theta}})$ is the vector of the Coriolis and centrifugal terms, and $\mathbf{G}(\boldsymbol{\theta})$ is the gravitational term. The joint torques at human upper-limb can be estimated by inverse dynamics when not wearing the device (right side in Figure 2.1):

$$\boldsymbol{\tau}_{Joint}^{without} = \boldsymbol{\tau}_{dyn}(\boldsymbol{\theta}, \dot{\boldsymbol{\theta}}, \ddot{\boldsymbol{\theta}}) \quad (2.3)$$

where $\boldsymbol{\tau}_{Joint}^{without}$ represents the joint torque without the device. On the other hand, the joint torques when wearing the device (left side in Figure 2.1) can not be determined due to redundancy of the torques ($\boldsymbol{\tau}_{joint} + \boldsymbol{\tau}_{assist}$).

$$\boldsymbol{\tau}_{Joint}^{with} + \boldsymbol{\tau}_{assist} = \boldsymbol{\tau}_{dyn}(\boldsymbol{\theta}, \dot{\boldsymbol{\theta}}, \ddot{\boldsymbol{\theta}}) \quad (2.4)$$

where $\boldsymbol{\tau}_{Joint}^{with}$ and $\boldsymbol{\tau}_{assist}$ represent the joint torque with the device and the supportive torque applied by the device.

2.2.2 EMG Measurements and Human Motion Analysis Wearing the Device

One approach to solve above issue is estimating joint torque from human EMG data using physiological models. The EMG readings indicate relative muscle activity.

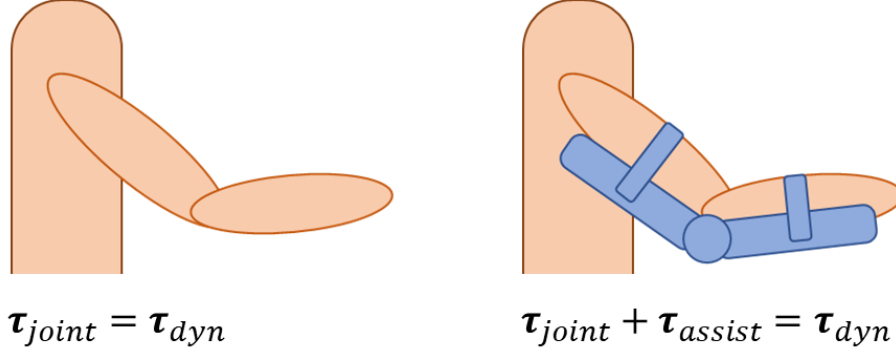


Figure 2.1: Example of upper-limb model.

Therefore, we estimated the torque from EMG data with a human model to clarify the supportive effect of the device. Note that torque estimation based on the human model in this research does not rely on the specific model of the device or the contact points between the device and the user. The device mass is only considered as a mass point at the corresponding position. The estimation procedure is as follows:

1. Human motions with and without the device are recorded, respectively, by using the motion-capture system and the EMG recordings.
2. $\tau_{dyn}(\theta, \dot{\theta}, \ddot{\theta})$ is calculated by performing inverse dynamics computation [36] in the scenario that the subject does not utilize the device.
3. EMG signals are converted to integral electromyogram (IEMG) [47] signals that are helpful for inferring muscular activity. τ_{Joint} is computed using the dynamics of the joint driven by several muscles as follows:

$$\tau_{Joint} = \sum_{i=1}^n e_i F_i l_i, \quad (2.5)$$

where e_i is a dimensionless IEMG value, which denotes the activity of muscle i (time-series data). e_i is generated from the EMG data once it is rectified and a band-pass filter is applied (lower cutoff frequency: 20 [Hz], upper cutoff frequency: 400 [Hz], interval of integration: 100 [ms]); then, it is normalized

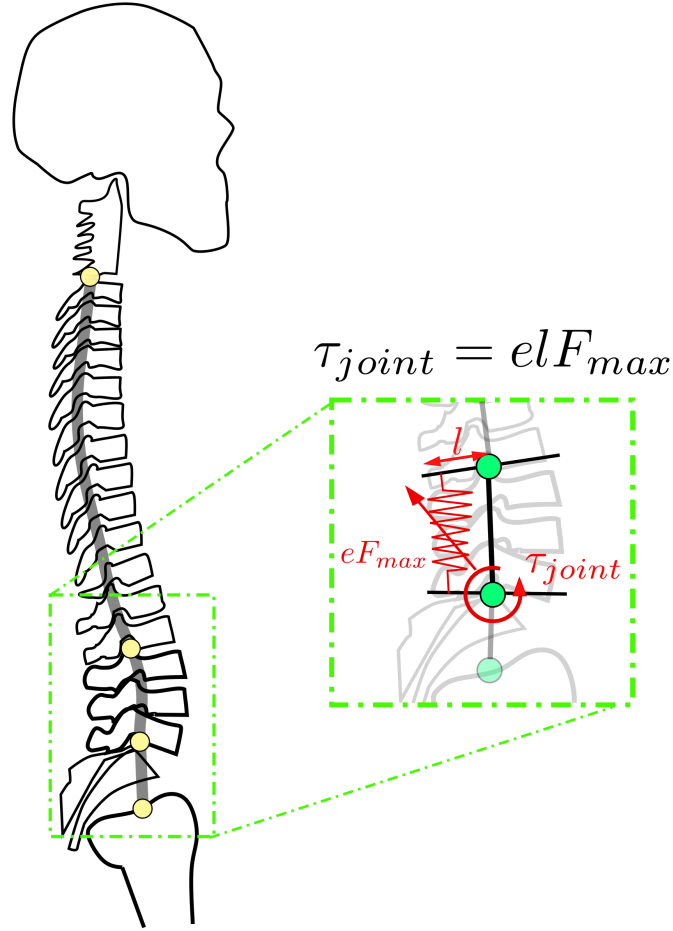


Figure 2.2: Simplified spinal muscular skeletal model.

by the maximum value, resulting in a e_i range of 0 to 1. F_i is the maximum muscle tension, and l_i is the moment arm of the lower back. In this study, the muscle tensions and moment arms were regarded unknown constants. According to Equations (2.1) and (2.5) with $\tau_c = 0$, $F_r l_r$, $F_l l_l$ were identified from EMG signals e_i and τ_{dyn} by using the least squares method in the case of motion data obtained without the device.

$$\begin{bmatrix} \tau_{dyn,t=0} \\ \vdots \\ \tau_{dyn,t=end} \end{bmatrix} = \begin{bmatrix} e_{r,t=0} & e_{l,t=0} \\ \vdots & \vdots \\ e_{r,t=end} & e_{l,t=end} \end{bmatrix} \begin{bmatrix} F_r l_r \\ F_l l_l \end{bmatrix}. \quad (2.6)$$

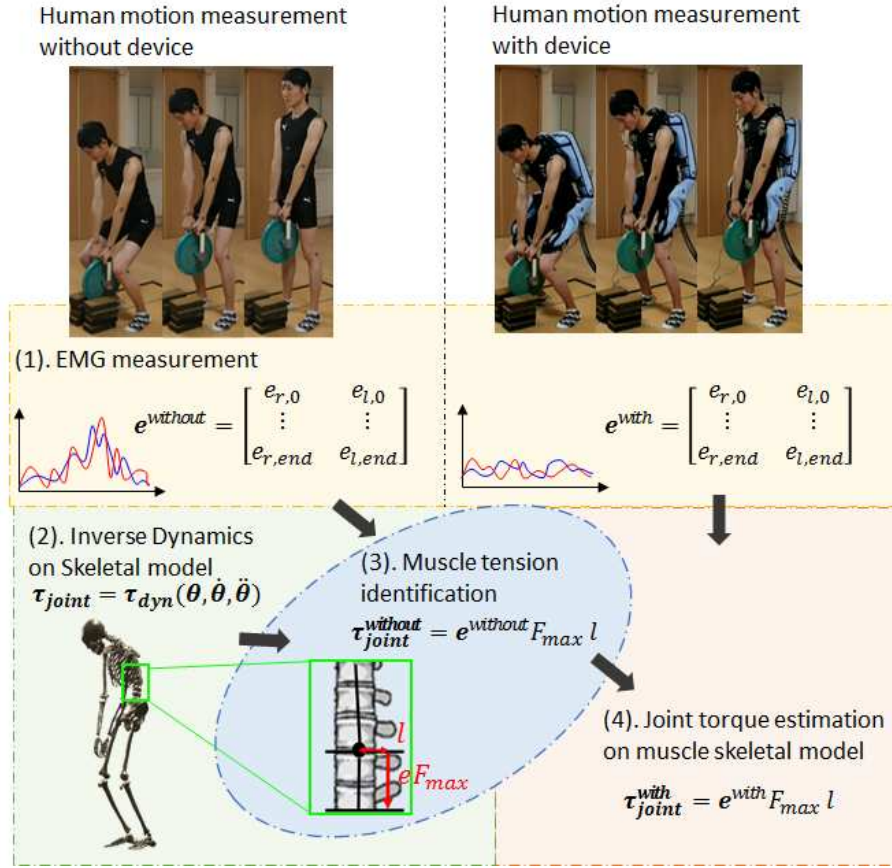


Figure 2.3: Overview of human motion experiment and muscle activity analysis.

4. The joint torque τ_{Joint} when wearing the device is estimated from the identified values $F_r l_r$, $F_l l_l$ and measured EMG signals using Equation (2.5). τ_{dyn} is also calculated as well for comparison with τ_{Joint} .

We tested this experimental method with a weight-lifting motion by using two different weights (5 and 10 kg). We measured EMG signals at two positions on the lower back (right and left erector spinae muscles).

2.3 Experimental Environment of Human Motion Measurement

In this study, we take the case that human uses a wearable assistive device as an example of human and device physical interaction. We analyze the human motion strategy when humans use a wearable assistive device. Here, we conduct the motion-measurement process used to gather data to extract the human motion strategy. In case of the human body, the joint state is corresponding to the muscle activity. Therefore, we analyze the muscle activities when utilizing the device and extract the strategy from measured data.

2.3.1 Assistive Device for Lower Back: Muscle Suit

In this experiment, we take the case of usage of the Muscle Suit [27] active assistive device herein, which supports the lower back with pneumatic actuators. The Muscle Suit shown in Fig. 2.4 was developed by Kobayashi et al. [27, 48] and commercialized by Innophys Co., Ltd., Tokyo [31]. The device is shaped like a backpack and is attached to the human body with a belt at the waist and soft pads at the thighs. When the pneumatic actuators on the device are contracted by supplying compressed air, the device powerfully lifts the upper body. The specific structure of the Muscle Suit is shown in Figure 2.4. The device has two joints around the waist joint to allow the human user to move naturally.

Figure 2.5 shows HRP-4 wearing the Muscle Suit. The robot can wear the device in exactly the same way as a human does: wearing on shoulders, attaching with the waist belt and thigh pads. The interface of the device is a touch switch or an exhalation switch, which controls the supply of the compressed air for driving the pneumatic actuators.

2.3.2 Measurement Setup for Human Motion

A snapshot of the motion-capture experiment is shown Fig. 2.6-(a). Motions performed using the assistive device were recorded using a motion-capture system

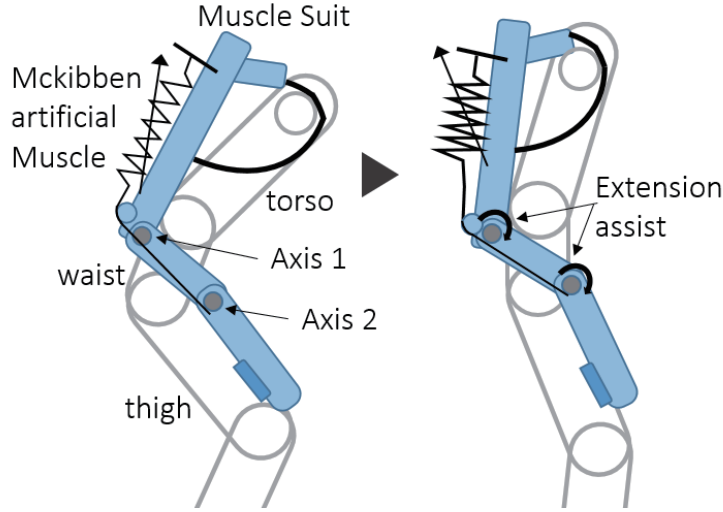


Figure 2.4: The specific structure of Muscle Suit

(Motion Analysis Corp., sampling rate: 200Hz).

Because Muscle Suit was designed for supporting motions involving lifting objects, we measured the human subject crouching down, holding a 5-kg weight, and then lifting it. We measured the same motion with a 10-kg weight as well. During the motion, we measured surface electromyogram (EMG) signals (DELSYS, sampling rate: 1000 Hz) from the lower back (erector spinae in the lumbar region), as shown in Fig. 2.6-(b). These EMG signals indicate muscular activity.

2.4 Muscle Activity analysis with Muscle Suit

In Figure 2.8, we show the estimated torque at the human lower back (for weight of 5 and 10kg). The blue line shows the result of τ_{dyn} estimated by inverse dynamics computation, and the red line shows the τ_{Joint} estimated using Equation (2.5) with IEMG signals during the weight-lifting motion when using the device.

The motion lasted approximately 4 s. The subject started lifting the weight at around 0.5 s and completed the motion at around 3.5 s, as in Figure 2.8. Although the torque computed from EMG data increased at the beginning of the motion at

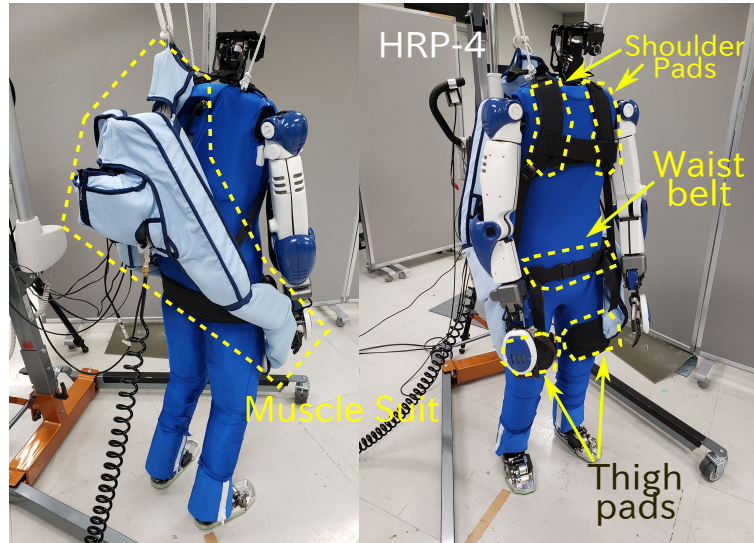


Figure 2.5: Humanoid robot HRP-4 and Muscle Suit. The device is attached on shoulders, waist, and thighs in exactly the same way as a human does.

around 0.5 s and at the end of motion at around 3.0 s, we observe that Muscle Suit drastically reduced the human joint torque between about 1 and 2.5 s. The joint was fully supported by the device, and the joint torque was nearly equal to zero, which gives us an assumption about human strategy utilizing the force intervention: the users wearing the assistive device try to take full advantage of the external force applied by the device and achieve the desired motion with less self-effort. In Figure 2.8, the ratios of torques from the EMG signals normalized against the maximum torque from inverse dynamics computation are 0.1186 ± 0.0605 (10 kg) and 0.0638 ± 0.0239 (5 kg). Given that negligible torque is observed in the period from the start of the motion to the end of motion, we can apply our method to the postures captured over this duration. Though these normalized values are small, we need to investigate the assumption that we can ignore such small torques when evaluating assistive devices with a humanoid robot.

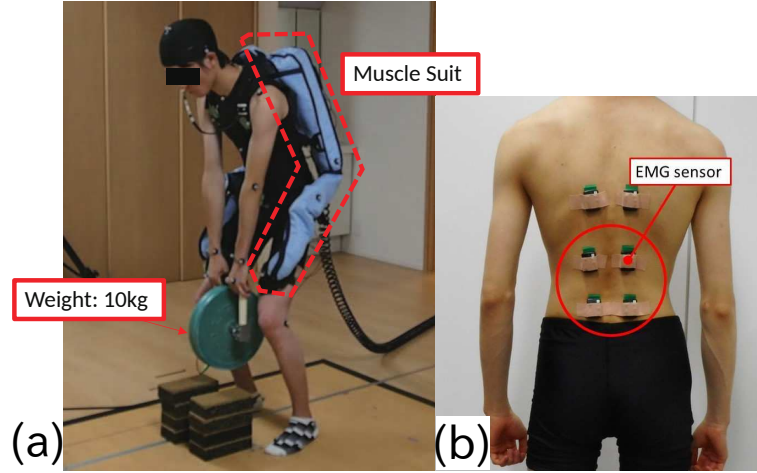


Figure 2.6: (a). Snapshot of experiment of human motion during equipment measurement; a human lifting a 10-kg weight by using “Muscle Suit”. (b). Placement of electromyography (EMG) measuring equipment.

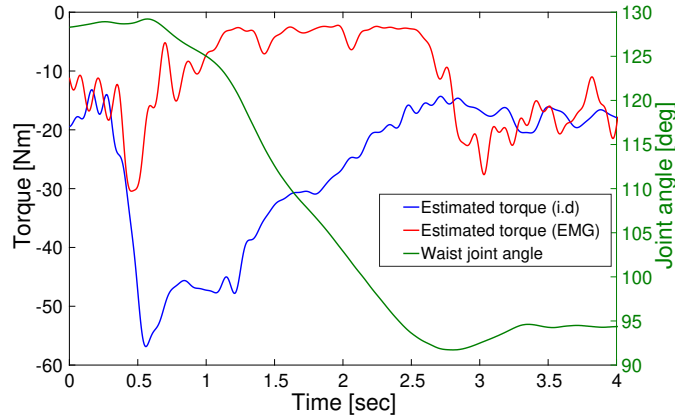


Figure 2.7: Estimated torque with 5 kg weight; the blue line shows τ_{dyn} estimated by inverse dynamics computation (i.d.), red line shows the τ_{Joint} estimated using Equation (2.5) with IEMG signals, and green line shows the waist joint angle.

2.5 Conclusion

In this chapter, we analyzed the human motion when using the wearable assistive device. We conducted the human subject experiment to measure the geometric

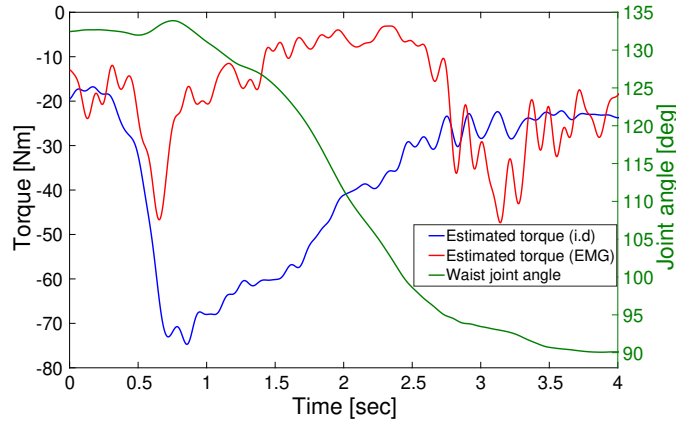


Figure 2.8: Estimated torque with 10 kg weight; the blue line shows τ_{dyn} estimated by inverse dynamics computation (i.d.), red line shows the τ_{Joint} estimated using Equation (2.5) with IEMG signals, and green line shows the waist joint angle.

motion trajectories and the human muscular activities under different conditions of using and not using the device. From the measured motion trajectories, the joint efforts on the human body was estimated as the torque values by inverse dynamics computation using the human skeletal model. The estimation of joint torques when utilizing the assistive device was achieved by analyzing the muscular activities measured as EMG signals and introducing the human musculoskeletal model. Finally, comparing the joint torques during the motion when using the device with that of not using the device, we assumed the human motion strategy of using the force intervention by the device.

From the result of this chapter, we assumed the human motion strategy using the force intervention: humans wearing the wearable assistive device try to take full advantage of the external force applied by the device and achieve the desired motion with less self-effort.

Chapter 3

Contact Estimator on Humanoid Robots for Observing Force Intervention

Previous chapter described the method to observe the force intervention on human body. In this chapter, we introduce the contact estimator to observe the force intervention applied by the device on humanoid robots.

The contact estimation on humanoid robot is used for necessary to execute the physical interaction between a robot and environment. Currently, our controller is not achieved to the human movements including multi-contact situation. To achieve more complex interaction situation, we introduce the practical contact estimation method in this section and will be combined in our controller in the future implementation.

Mostly, the contact estimation provides the information including contact detection, contact force identification and contact point localization [49, 50, 51]. In contact detection and identification part, our estimator determines if there is a contact and computes its strength in terms of force wrench. Then, in the contact point localization part, we estimate the contacted link and the point on body surface of robot 3D model where the contact occurred.

3.1 Contact Estimation on Humanoid Robot

3.1.1 Contact Detection and Identification

For humanoids, by observing the forces at their floating body, we can obtain the force acting on the robot. A humanoid dynamic model can be written as:

$$\mathbf{M}(\mathbf{q})\ddot{\mathbf{q}} + \mathbf{C}(\mathbf{q}, \dot{\mathbf{q}})\dot{\mathbf{q}} + \mathbf{G}(\mathbf{q}) = \boldsymbol{\tau}_m + \sum_{i=1}^{n_c} \mathbf{J}_i^T \mathbf{F}_i + \boldsymbol{\tau}_\delta, \quad (3.1)$$

where \mathbf{q} is the generalized joint coordinates consisting of linear position, orientation of the floating body or base and the joint angles. $\mathbf{M}(\mathbf{q})$ is the inertia matrix, $\mathbf{C}(\mathbf{q}, \dot{\mathbf{q}})$ is the matrix including centrifugal and Coriolis effect, $\mathbf{G}(\mathbf{q})$ is the vector of gravitational term. $\boldsymbol{\tau}_m$ is the vector of joint torque, $\mathbf{J}_i^T \mathbf{F}_i$ is the desired contact forces which \mathbf{J} is the contact Jacobian and \mathbf{F} is the contact force measured by force/torque sensors, and $\boldsymbol{\tau}_\delta$ is the undesired external contact force that we estimate.

Since base link has no actuated joints, the dynamics equation can be written by the following decomposed form,

$$\begin{aligned} & \begin{pmatrix} \mathbf{M}_b(\mathbf{q}) & \mathbf{M}_{bj}(\mathbf{q}) \\ \mathbf{M}_{jb}(\mathbf{q}) & \mathbf{M}_j(\mathbf{q}) \end{pmatrix} \begin{pmatrix} \ddot{\mathbf{q}}_b \\ \ddot{\mathbf{q}}_j \end{pmatrix} + \begin{pmatrix} \mathbf{C}_b(\mathbf{q}, \dot{\mathbf{q}}) \\ \mathbf{C}_j(\mathbf{q}, \dot{\mathbf{q}}) \end{pmatrix} \begin{pmatrix} \dot{\mathbf{q}}_b \\ \dot{\mathbf{q}}_j \end{pmatrix} + \begin{pmatrix} \mathbf{G}_b(\mathbf{q}) \\ \mathbf{G}_j(\mathbf{q}) \end{pmatrix} \\ & = \begin{pmatrix} \mathbf{0} \\ \boldsymbol{\tau}_m \end{pmatrix} + \sum_{i=1}^{n_c} \mathbf{J}_i^T \mathbf{F}_i + \begin{pmatrix} \boldsymbol{\tau}_{\delta, \text{base}} \\ \boldsymbol{\tau}_{\delta, \text{joint}} \end{pmatrix}. \end{aligned} \quad (3.2)$$

In Equation (3.2), we focus on the equation of the base link and estimate the undesired contact force acting on base link as:

$$\boldsymbol{\tau}_{\delta, \text{base}} = - \sum_{i=1}^{n_c} \mathbf{J}_{i, \text{base}}^T \mathbf{F}_i - \boldsymbol{\tau}_{\text{dyn}}, \quad (3.3)$$

where $\mathbf{J}_{i, \text{base}}$ is a Jacobian of the force sensor link to the base link, $\boldsymbol{\tau}_{\text{dyn}}$ is the left side of Equation (3.2) at the base link.

In Equation (3.3), $\boldsymbol{\tau}_{\delta, \text{base}}$ consists of the linear force part $\boldsymbol{\tau}_{\delta, \text{base}}^v$ and rotational torque part $\boldsymbol{\tau}_{\delta, \text{base}}^\omega$. We assume that most contacts mainly apply the linear force

to robot and the torque part can be ignored as $\boldsymbol{\tau}_{\delta, \text{base}}^{\omega} = \mathbf{0}$. From the norm of the estimated contact force $\boldsymbol{\tau}_{\delta, \text{base}}^v$ in Equation (3.3), we can detect the contact by thresholding the force:

```

if ( $\|\boldsymbol{\tau}_{\text{delta,base}}^v\| > f_{\text{threshold}}$ ) then
    ContactDetected  $\leftarrow$  true
else
    ContactDetected  $\leftarrow$  false
end if

```

After detecting the contact, we can simply estimate the contact force strength as $\boldsymbol{\tau}_{\delta, \text{base}}^v$. Through the above procedure, we can detect the contact and identify the contact force strength at the same time.

3.1.2 Contact Link and Point Estimation

Once contact is detected, we search the contact link by inspecting the error torque $\tau_{\delta, i}$ along the kinematic chain of the robot. The contact link searching is done by simple depth-first search algorithm, which inspects whether the error torque is higher than the threshold from the base link to distal links. Figure 3.1 shows the contact link searching algorithm. Since the successor joint torque cannot be affected by the predecessor joint torque, the link attached to the most distal joint containing the error torque is the link in contact. In Figure 3.1, let us assume that the contact force is applied to link l_{i+2} the contact force generates the error torque τ_{i+2} at self-joint and every predecessor joint until the base link but no error torque is generated at the links in another branches like link l_j , l_m or l_n . When the contact link is found, the contact point can be estimated by computing the intersection between the convex hull or the mesh from the robot 3D model and the line of action of contact force.

When the contact force is applied to the contact link, both contact force and link are now known as a result of the previous step. Now, the external forces due to the contact force can be written with an unknown Jacobian to contact point.

$$\boldsymbol{\tau}_{\delta} = \mathbf{J}_C^T \mathbf{F}_C, \quad (3.4)$$

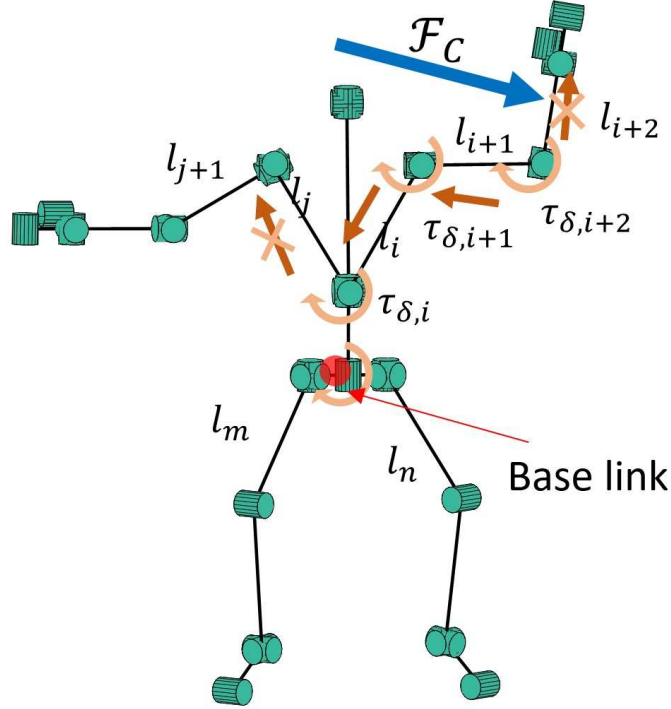


Figure 3.1: Contact link searching algorithm. The contact force is applied to link l_{i+2} the contact force generates the error torque τ_{i+2} at self-joint and every predecessor joint until base link but no error torque is generated at the links in another branches like link l_j , l_m or l_n . Tracing the link containing the error torque, the contact link can be found. where \mathbf{J}_C^T is a Jacobian of the unknown contact point \mathbf{x}_C expressed in local frame of its link, and \mathbf{F}_C is the local frame representation of $\boldsymbol{\tau}_{\delta,\text{base}}^v$ ($\mathbf{F}_C = R_c^T \boldsymbol{\tau}_{\delta,\text{base}}^v$).

In order to reconstruct the line of action, we can replace the unknown Jacobian \mathbf{J}_C on the contact link with known geometric Jacobian $\mathbf{J}_{t,i}$ and $\mathbf{J}_{r,i}$ for the linear and the rotational velocity respectively,

$$\mathbf{J}_C = \mathbf{J}_{t,i} - [\mathbf{x}_C \times] \mathbf{J}_{r,i}, \quad (3.5)$$

where, $[\ast \times]$ denotes the skew-symmetric matrix representation instead of the cross product operation. From Equation (3.4) and Equation (3.5), we obtain the follow-

ing equation,

$$\begin{aligned}\boldsymbol{\tau}_\delta &= (\mathbf{J}_{t,i} - [\mathbf{x}_C \times] \mathbf{J}_{r,i})^T \mathbf{F}_C. \\ &= (\mathbf{J}_{t,i} \mathbf{F}_C - \mathbf{J}_{r,i})^T [\mathbf{F}_C \times] \mathbf{x}_C.\end{aligned}\quad (3.6)$$

Although the contact point \mathbf{x}_C is unknown in Equation (3.6), the line of action can be reconstructed by the following equation,

$$[\mathbf{F}_C \times] \mathbf{x}_C = -(\mathbf{J}_{r,i})^\dagger (\mathbf{F}_C - \mathbf{J}_{t,i})^T \mathbf{F}_C, \quad (3.7)$$

where \dagger denotes the pseudo-inverse operation. While Equation (3.7) has three equations, only two equations are effective to compute the contact point \mathbf{x}_C due to rank deficit of the skew-symmetric matrix.

We use the triangular mesh generated from robot 3D CAD model to find the contact point as an intersection between the line of action and the triangular mesh¹ (i.e. check the intersection of the action line with each triangle composing a given link). We then can have zero or multiple intersections. In the case of no intersection, the considered link is not in contact for the given link. In the case of intersection, the contact point is found. If there are more than two, one of them is chosen by considering the robot posture. We can use the convex hull to avoid this conflict of multiple intersections yet, using the polygon mesh directly triangulated from 3D CAD model gives more precise contact points.

In the next section, we use external torque estimation in this method to extract the assistive torque applied by the device. The contact link detection and point localization procedure will be used in future implementation.

3.2 Experimental Validation of Contact Estimation

We implemented our contact estimation method on our humanoid robot HRP-4 to assess its feasibility. In this section, the contact detection and the contact point

¹Clean triangular meshes can be obtained from points or polygons using CGAL library.

estimation on simulated humanoid is shown then the same procedure is ported on the real humanoid hardware, and the results are also shown. We apply a single contact force to the robot. Although our method can be applied to the dynamic situation, dynamic case is left for future works and only the static case is shown in this study.

3.2.1 Contact Estimation in Simulation

Before we implemented our contact estimator on the real robot, we have investigated its performance in simulation. In this experiment, we apply the force to a simulated humanoid and confirm whether the contact detection and point estimation can be correctly achieved.

The contact forces are applied to left and right elbow link as shown in Figure 3.2. The direction of the applied force at left elbow link is fixed, whereas it is moving when applied at the right elbow link. The forces for both links are pulling forces, which contact points are fixed. The force strength is approximately 25 to 30 N, which is applied continuously during 8 sec and 18 sec respectively.

The result of the experiment in simulation is shown in Figure 3.3 with identified contact force strength that is norm of contact force in Equation (3.3) (left y -axis) and contact detected link index (right y -axis). According to the result, the contact is detected at left elbow link indicated as link index No. 30 in Figure 3.3 from 2 sec to 12 sec then it is detected at the right elbow link (link index No. 21) from 22 sec to 40 sec.

When the contact link is detected, a line of action of the contact force is reconstructed and used to compute the contact point. The latter is the result of the intersection between the reconstructed line of action and the robot's link polygon meshes. The reconstruction of the line is derived by Equation (3.7) in Section 3.1.2. For generating the polygon meshes of robot links, we used the 3D point set of the CAD model. The outcome is a list of triangles. Thus, the contact points are computed as intersections between lines and each triangle. As a result, we can have one or more points pulling (force vector goes out from robot body) and

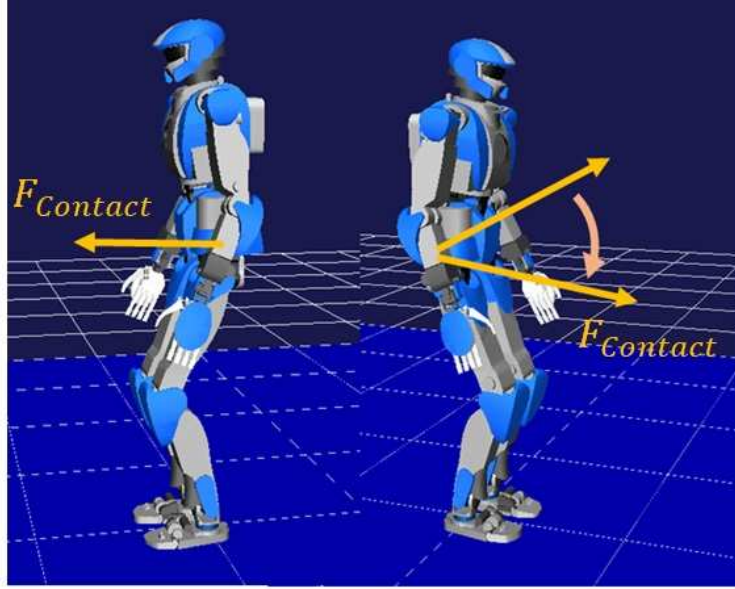


Figure 3.2: Applying a single force to left and right hands in simulation. The force applied to left elbow link is fixed and the direction of the force applied to right arm is moving down.

pushing away (force vector goes in to robot body). In case where more than two contact points computed, we can chose one of them, considering the task the robot is doing or the environment surrounding the robot, otherwise, we chose the closest one to the initial point of the reconstructed line (segment) because most of contact force vector is pushing away unless the body is hung on something.

Figure 3.4 shows the body mesh, reconstructed lines and contact points marked on body surface. Contact points are not always found due to the accuracy of the reconstructed line of action. Each line is depicted at 250 ms intervals. In Figure 3.3, read marks “x” are placed when the contact points are found. During 3 sec to 8 sec in Figure 3.3, the reconstructed lines are stable and always going across a mesh, therefore, the contact points are correctly computed on the elbow link surface. In the case of right arm during 22 sec to 40 sec, the lines are reconstructed however, some of them are not going across a mesh, which is caused by a mismatch of the reconstructed line. Even in the case where the contact link detection is correctly done, the contact point estimation may have failed due to inaccuracy in

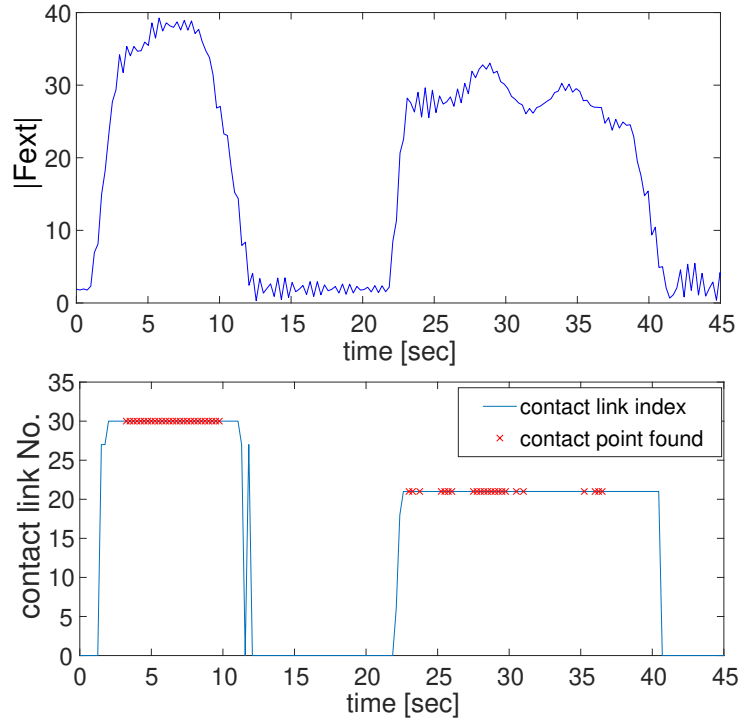


Figure 3.3: Result of contact link detection, force strength identification and contact point estimation in simulation. Upper part indicates force strength of contact force and lower part indicates the contact link index (No. 21 is right elbow link, No. 30 is left elbow link).

the robot state estimation. Even in simulation, contact forces resulting from virtual pushes may have numerical issues sometimes and this may cause such failures. This problem is discussed in the experiments conducted on the real humanoid (see next section). In both cases however, the contact link is detected and the direction of the line of action is correctly reconstructed.

3.2.2 Contact Estimation on the Real Humanoid Robot and Practical Discussions

We apply the same method to the real humanoid robot setup to assess both the feasibility and performance of the proposed estimator on a real hardware. Com-

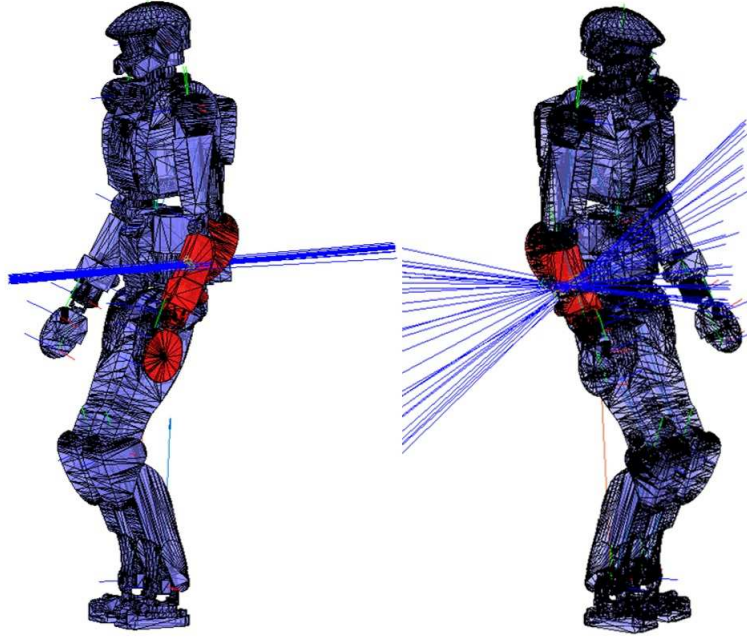


Figure 3.4: Reconstructing a line of action of contact forces and computing the intersections between a line and the robot body mesh. Right side figure shows the result of the left elbow link and the left side shows that of the right one. The detected contact links are highlighted in red.

paring the real robot with the simulated one, there are many differences such as the sensor noise, the joint flexibility and the friction problems. Thus, how these problems affect the estimator is discussed in the end of this section.

We use the human-sized humanoid robot HRP-4 that height and weight is 155 cm and 40 kg respectively. The robot has 9 degrees of freedom (dofs) (shoulder: 3 dofs, elbow: 1, wrist: 3, hand: 2) in each arm, 7 dofs in each leg (hip: 3, knee: 1, ankle: 2), 3 dofs in chest, 2 dofs in neck and total dofs is 37. HRP-4 is position-based controlled robot with high PD gains; it has an accelerometer and gyroscope mounted at the base link for base link state estimation, encoders mounted at each joint for joint angles \mathbf{q} and joint angular velocity $\dot{\mathbf{q}}$, current sensors mounted at each joint for joint torque $\boldsymbol{\tau}_m$, 6-axis force/torque sensor mounted at each foot link for floor reaction force.

In this experiment, we apply a single force to the right elbow link (Figure 3.5(a).), right shoulder link (Figure 3.5(b).), left elbow link (Figure 3.5(c).), left shoulder link (Figure 3.5(d).) in this order. Figure 3.5 depicts the position where the force is applied and the direction of the force. The direction of the applied force to right and left elbow links is almost similar to the direction of the applied force to right and left shoulder links as shown in Figure 3.5. During the experiment, we measured the applied force strength by a 1-axis force gauge so that we can compare it with the estimated force.

The Figure 3.6 shows the result of contact link detection and force identification. The estimated contact force is shown with a solid-line and the measured contact force by force gauge is drawn with a dashed-line. In Figure 3.6, first, we apply the force to right elbow link (Figure 3.5(a).) although the shoulder link is detected. One of the reason that the contact link is mismatched with the expected one is considered due to the joint friction or high stiffness due to a high proportional gain for the feedback control. Because the gear ratio of the elbow joint is very high, the static friction is therefore also high, reducing the torque caused by the contact force. As a result, the contact is detected at shoulder link that is the predecessor link of the elbow link. Although the contact detection failed, the contact force is successfully estimated. The contact link detection and contact force estimation are independent in the way they are processed. Thus, there are cases where one of them is correct even if the other is not. Next, about 30 N of the force is applied to the right shoulder link (Figure 3.5(b).) at around 30 sec in Figure 3.6. In this period, the contact link detection succeeded, however, the estimated contact force has a bias error by about 7 N. Another force is then applied to the left elbow link (Figure 3.5(c).) but the left shoulder link is detected, similarly to right elbow case. The contact force estimation succeeded as its strength is similar to the measured one. Finally, we apply the force to the left shoulder (Figure 3.5(d).). Similarly to the right link case, the contact link detection succeeded. However, we observed a difference of approximately 5 N between the estimated and measured force.

In the real robot experiment, the contact point is not found due to the incorrect link detection or an inaccuracy of the error torque τ_δ at each joint. Even in the

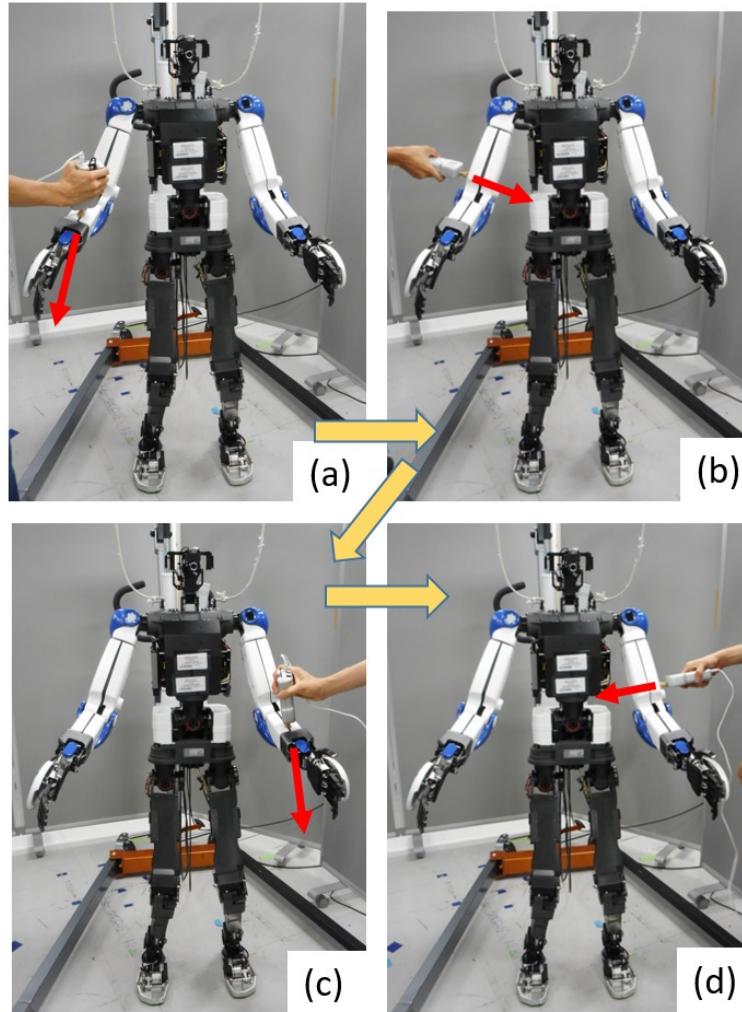


Figure 3.5: Applying a single force to right and left arms in HRP-4. The force was applied to right elbow link (a), right shoulder link (b) then, left elbow link (c), left shoulder link (d) by fixed direction.

case where the estimator detects an incorrect link, if that link is the predecessor link of the correct one, it might be possible to find a contact point by using the mesh associated with that of the successor link. For instance, in the previous experimental result, using the joined body mesh of the right shoulder link and elbow link instead of using the single body mesh of the right shoulder might allow to find the contact point. Therefore, it is better to use all links of a given tree to

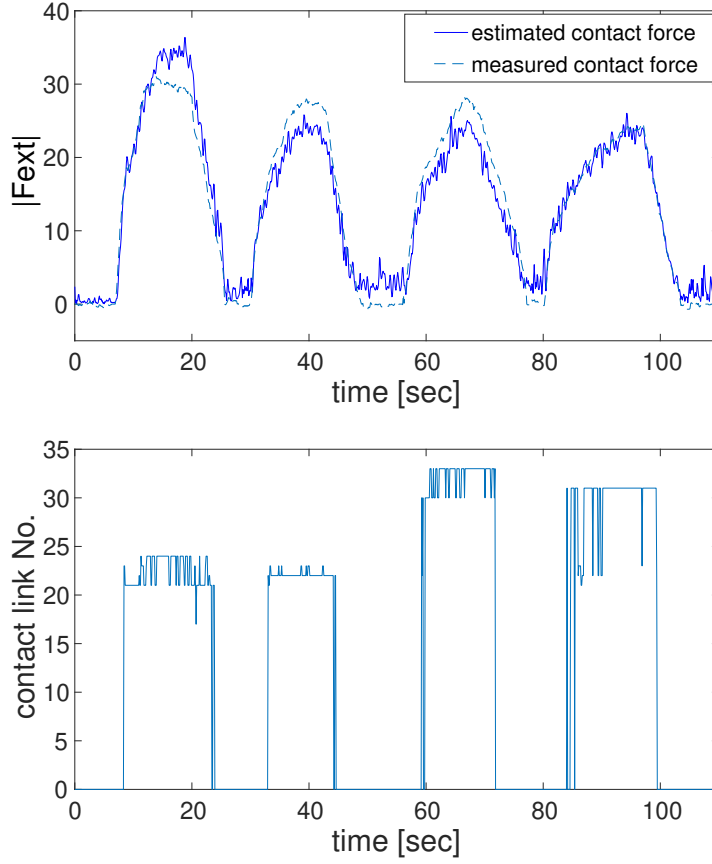


Figure 3.6: Result of contact link detection, force strength identification and contact point estimation in HRP-4. Left y -axis indicates the force strength of contact force and right y -axis indicates the contact link index (No. 21-23 is right shoulder link, No. 24 is right elbow link, No. 30-32 is left shoulder link and No. 33 is left elbow link).

choose the best match. In Figure 3.7, the joined body mesh of left shoulder and elbow link is shown in red mesh. Some of the reconstructed line are going across the joined body mesh, which give the intersections as a result. Determining the threshold for each joint based upon the joint stiffness instead of using is unique value is one of the possible solutions for avoiding mis-detection.

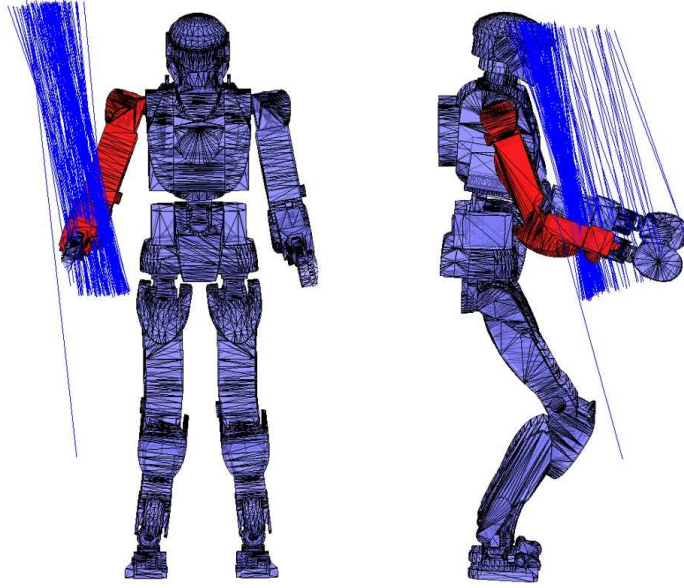


Figure 3.7: Reconstructing a line of action of contact forces and computing the intersections between a line and the joined body mesh. The joined body surface of left shoulder link and elbow link are shown in red. Right side figure shows the result of left link and left side shows that of right one.

3.3 Conclusions

In this chapter, we proposed a contact estimation method for a humanoid robot that allows to identify the contact force strength, detect the contact link and estimate the contact point by using the meshes of the robot body. The contact force identification can be performed by computing the error between the generalized forces estimated from the expected robot state and those measured from the real robot sensory data. The estimator can basically provide the resultant forces which allow to detect reliably single contact force. Extension to multiple contact forces is possible by tracing the joint torques of all tree and achieving the total wrench force distribution weighted by the excess of torques. For the contact link detection, the contact link is similarly derived by tree search method using robot kinematic chains. Finally, after reconstructing the line of action of the contact force, the

contact point is estimated as intersection between the reconstructed line and the triangles composing the mesh of the link or its convex hull.

The contact point estimation succeeded when applying the external force with almost time-constant force strength value and fixed direction; on the other hand, it failed when applying the force with time-varying strength value and direction. This issue needs to be investigated further. In the real robot experiment, the accuracy of the estimated contact force strength was depending on the link where the external force is applied, or on the direction of the applied force. The contact point estimation is not perfect on the real robot, which may be caused by the following two different issues. One of the two is that misdetection of the contact link. In this case, obviously, the intersection cannot be found because the line does not cross the link's mesh. The other issue is the inaccuracy of the estimated error torque that produced by the contact force. As the error is computed from the inverse dynamics computation of the robot model, the latter problem is due to the modeling error about the inertial parameter of the robot. However, this error can be improved by a re-identification of the inertial parameter [52, 53]. Adding the joint friction model to the robot dynamics equation also might improve robustness and precision. Those issues will be considered in our future works, together with the extension of our method to the multiple contact situation and the dynamic motion case.

Chapter 4

Human Motion Reproduction of Assistive Device Usage on Humanoid Robot

4.1 Introduction

In this chapter, we propose a humanoid controller that reproduces human motions supported by the powerful active devices. We focus on the devices supporting human lower back which is the most common type among those commercially available in Japan. The proposed controller is based on assumptions about how humans behave when using an active device, namely that humans follow nominal trajectories, and that they try to move with least effort by taking advantage of external supportive forces. The major outcome of this study is the novel humanoid controller that interacts with external forces generated by an active device while tracking retargeted human motions. The control scheme is realized by tracking the trajectory of measured human motion with torque feedback. The proposed control framework is validated by experiments to evaluate the supportive torque of a powerful assistive device “Muscle Suit” [31] by using the humanoid HRP-4.

This chapter is organized as follows. After arguing assumptions behind the behavioral intentions of human motions when supported by wearable devices, and the

proposed a novel control scheme is described based on these assumptions in Section 4.2. Section 4.3 presents the experimental validation of the proposed control scheme using the humanoid HRP-4 to evaluate the Muscle Suit before concluding the chapter.

4.2 Torque-based Human-motion Tracking Control

4.2.1 Assumptions of Human Behavior with Assistive Devices

To design the humanoid motions similarly to human motions, we made the following assumptions about human behavioral intention when they benefit from the external force of active assistive devices.

Assumption 1

A wearable assistive device gives geometric constraints to the human body in such a way that the resulting human motions track almost the nominal trajectories.

Assumption 2

The user takes full advantage of the supportive effect of the assistive device and moves with less effort.

The first assumption comes from the structural constraints of assistive devices. Since the devices are designed for supporting a typical human task such as lifting an object, the resultant user motions are likely to follow an identical trajectory because they are guided by the mechanical structure of the device. The motion trajectory for the humanoid robot is generated by using the retargeting method [54] from the recorded human motion. It is natural to make the second assumption; when our motion is supported by powerful assistive devices, we tend to move with smaller effort and rely on the external force coming from the device. The

assumption is verified in Chapter 2. Based on our assumptions, we propose a path tracking control based on torque feedback (described in 4.2.3) after we show how to generate the humanoid motion trajectory from measured human motion trajectories.

4.2.2 Human Motion Retargeting for Humanoid

Our control framework needs to track the joint trajectory that is sufficiently close to that of humans'. Motion retargeting is a technique that is often utilized to generate human-like motions of a computer graphics character or a humanoid robot. In this study, the tracked trajectories are designed by the efficient motion retargeting method for humanoid robots, which is detailed elsewhere [54]. Since the method makes use of the geometric parameters identification, it can cope with the differences of body dimensions between a human and a robot. It can also consider physical consistency such as conditions regarding joint limitations or balancing.

In our case, as the robot needs to wear an assistive device while carrying weights, we set the motion retargeting procedure as follows:

1. The motion of a human subject wearing an assistive device is measured by a motion capture system.
2. The simulation model of a robot is modified to reflect the same load conditions in the human measurement. The masses of the device and the carried weights are added as the mass point models.
3. The robot motion is retargeted from the measured human motion by utilizing the simulation model, according to the method shown elsewhere [54].

Finally, the retargeted motion trajectory is sent to the robot as whole joint trajectories for the tracking control that we describe below. Human motions wearing the device are used for retargeting here because we believe it is important to evaluate the assistive torque under the situation as close as the real use. We will discuss this issue later in the conclusion.

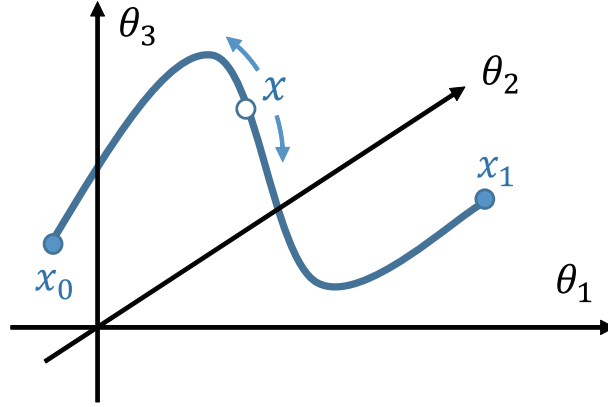


Figure 4.1: Relationship between joint angle trajectory and a trajectory parameter x (ex. 3DOFs). Each value of $\theta_i (i = 1, 2, 3)$ is derived from the one-by-one mapping function $\boldsymbol{\theta}(x)$: $[\theta_1 \ \theta_2 \ \theta_3]^t = \boldsymbol{\theta}(x), x_0 \leq x \leq x_1$

4.2.3 Path Tracking Control with Joint Torque feedback

In order to reproduce human motion when an external force is applied from the assistive device, we introduce a single coordinate representation of multiple joints and the path tracking control in a similar manner to the method shown in [55, 56]. In this scheme, the retargeted motion trajectory of the humanoid robot is represented by a single parameter and utilized for path tracking control. The whole joint angle trajectories of a robot are represented by a single scalar parameter x , which is called the trajectory parameter in the path coordinate. As an example, the case of a three dimensional trajectory is shown in Fig. 4.1. The current joint angles are represented by $\boldsymbol{\theta}(x)$, where $\boldsymbol{\theta}(x)$ is a one-by-one mapping function from trajectory parameter x to current joint angles $\boldsymbol{\theta}$. Since the retargeted motion mentioned in the previous section is often given as discrete data, the mapping function can be designed by the trajectory interpolation.

When the joint angles of a robot are constrained under the mapping function $\boldsymbol{\theta}(x)$, the equation of motion of a robot can be written as follows:

$$\tau_{joint} + \tau_{ext} = f(x) \triangleq h(\boldsymbol{\theta}(x), \dot{\boldsymbol{\theta}}(x), \ddot{\boldsymbol{\theta}}(x)) \quad (4.1)$$

where τ_{joint} and τ_{ext} are the joint torque and external torque, respectively, and

$f(x)$ or $h(\boldsymbol{\theta}(x), \dot{\boldsymbol{\theta}}(x), \ddot{\boldsymbol{\theta}}(x))$ indicate the torque coming from the inertial, Coriolis, and gravity forces respectively.

Let us now define the following error torque at the joint, where it is supported by the device:

$$e_\tau \triangleq \tau_{ref} - \tau_{joint} \quad (4.2)$$

where τ_{ref} indicates the reference joint torque. According to our assumptions, τ_{ref} should be zero, or has a negligible value, to perform the motion with less self-joint torque. Now, we regard τ_{ref} as a small constant value:

$$\ddot{e}_\tau + K_1 \dot{e}_\tau + K_2 e_\tau = 0 \quad (4.3)$$

where K_1 and K_2 ($K_1 > 0, K_2 > 0$) are feedback gains. Since τ_{ref} is constant, Equation (4.3) can be written as

$$-\frac{d}{dt} \dot{\tau}_{joint} - K_1 \dot{\tau}_{joint} + K_2 (\tau_{ref} - \tau_{joint}) = 0 \quad (4.4)$$

Here, we assume that the external torque acting on the robot changes slowly with respect to the dynamics of the robot, such that τ_{ext} is quasi-static and is regarded as constant. From this assumption, $\dot{\tau}_{joint}$ can be computed from Equation (4.1) as follows:

$$\dot{\tau}_{joint} = \dot{f}(x) = \frac{\partial f}{\partial x} \dot{x} \quad (4.5)$$

By substituting Equation (4.5) onto Equation (4.4) and utilizing Laplacian operator s , we can get:

$$-(s + K_1) \frac{\partial f}{\partial x} \dot{x} + K_2 (\tau_{ref} - \tau_{joint}) = 0 \quad (4.6)$$

$$(4.7)$$

Then, \dot{x} is represented as:

$$\dot{x} = \frac{K_2}{s + K_1} \left(\frac{\partial f}{\partial x} \right)^{-1} (\tau_{ref} - \tau_{joint}) \quad (4.8)$$

Finally, we obtain acceleration \ddot{x} along the path coordinate as:

$$\ddot{x} = -K_1\dot{x} + K_2 \left(\frac{\partial f}{\partial x} \right)^{-1} (\tau_{ref} - \tau_{joint}) \quad (4.9)$$

If path coordinate x is updated according to Equation (4.9), the feedback control rule written in Equation (4.3) will be satisfied.

4.3 Experiments

This section presents experimental results to verify our proposed framework. The experimental setup with the pneumatic exoskeleton Muscle Suit and the full-size humanoid robot HRP-4 is first introduced in 4.3.1. The proposed control method is then applied to the setup and the experimental results of the generated motion are shown in 4.3.2.

4.3.1 Experiment Setup

In this experiment, we also use the device Muscle Suit which is explained in Section 2.3.1. The structure of the Muscle Suit is also shown in Fig.2.4. It was designed to help human carry heavy objects by supporting the lower back. The device has McKibben pneumatic actuators on the backside, which are driven by compressed air. It is designed like a backpack so that a user can easily put on and take off the device. The device is fixed and tightened by a belt at the shoulders, and the thighs are supported by soft pads. The waist joint of the Muscle Suit consists of two joints that allow natural human motions. The user can control the amount of supplied air to the pneumatic actuators by using a touch switch, or an exhalation switch so that it can be controlled during the tasks requiring both hands.

Fig. 4.2 shows the human-sized humanoid robot HRP-4 [57] used for device evaluation in this study. Its geometric parameters, such as the link lengths are designed to be similar to the average values of Japanese females, within an error range of 10%, and its height and weight is 155 cm and 40 kg respectively. This humanoid robot with the similar body dimensions to a human makes it easy to

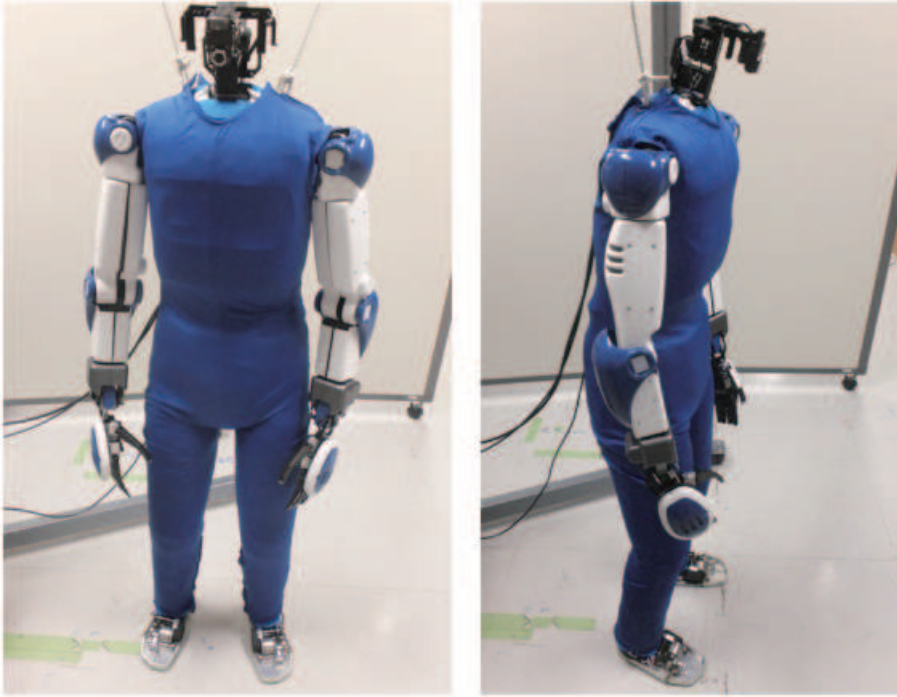


Figure 4.2: Humanoid HRP-4 (softcover)

imitate human-like motions. The total number of degrees of freedom (DOFs) of the robot is 37. Each arm has 9 DOFs (shoulder joint: 3, elbow: 1, wrist: 3, hand: 2), each leg has 7 DOFs (hip joint: 3, knee: 1, ankle: 2, toe: 1), the waist has 3 DOFs, and the neck has 2 DOFs. The original hard plastic cover of HRP-4 is replaced by soft urethane to allow it to wear the assistive device as humans do without any modification.

4.3.2 Experiment of Proposed Control Scheme

Since the proposed controller requires retargeted human motion trajectories, we first measured the human motion with a motion capture system. In the measurement, the subject lifted a 5-kg load while wearing the Muscle Suit, as shown in Fig. 4.4 (upper side). The subject bent down and held a 5-kg weight then lifted the weight with supportive force from the device, while using the exhalation switch

to activate the device. During the motion, the motion trajectory was captured by several motion capture cameras (Motion Analysis). The joint trajectories of a humanoid robot were generated from the measured human motions using the procedure mentioned in 4.2.2. The obtained trajectories were used as $\theta(x)$ in our control scheme.

We now detail the implementation of our controller in the experiments. Since the Muscle Suit was designed to support the human lower back, we focused on the waist joint torque of the humanoid. For real-time control, the upper-body dynamics of the robot were simplified by a quasi-static inverted pendulum model. The function $f(x)$ in Equation (4.1) was formulated as follows:

$$f(x) = mgl \sin(\theta_{waist}(x)) \quad (4.10)$$

where θ_{waist} is the waist joint angle, m is the total mass of the upper body, g is the acceleration due to gravity, and l is the relative distance between the waist joint position and the center of the total mass of the upper body.

We then differentiate Equation (4.10) with respect to the trajectory parameter x :

$$\frac{\partial f}{\partial x} = mgl \cos(\theta_{waist}) \frac{\partial \theta_{waist}}{\partial x} \quad (4.11)$$

In the actual implementation, Equation (4.9) was discretized. We also considered that τ_{ref} is equal to 0 so that the robot could put its upper-body weight onto the assistive device as much as possible. Finally, Equation (4.9) was reformulated as follows:

$$\begin{cases} x[t+1] = x[t] + \dot{x}[t]\Delta t & (0 \leq x \leq 1) \\ \dot{x}[t] = K_1 \dot{x}[t-1] \\ \quad - K_2 \left(mgl \cos(\theta_{waist}) \frac{\partial \theta_{waist}}{\partial x} \right)^\dagger \tau_{joint} \end{cases} \quad (4.12)$$

where, $*^\dagger$ means the singular robust (SR) inverse [58]. τ_{joint} is measured by current sensor attached to the motor of the waist joint of HRP-4.

The above controller was tested on the humanoid robot HRP-4 wearing the Muscle Suit. In the experiment, we attached a total weight of 4-kg onto the robot

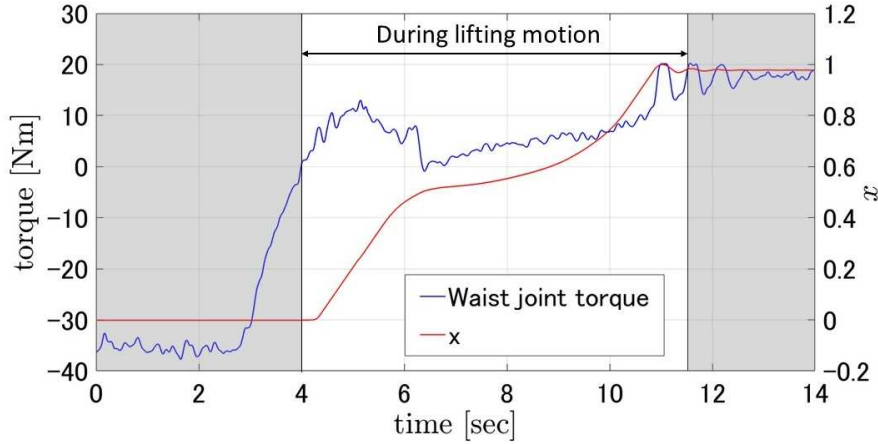


Figure 4.3: Waist joint torque and velocity of parameter x ($0 \leq x \leq 1$). The robot motion starts at 4 [sec] when the waist joint torque becomes zero. The motion is maintained for 7 s and ends at around 11 s.

(2-kg weights on each wrist). The maximum value of air pressure supplied to the device was set to 0.3 MPa (standard pressure supply: 0.5 MPa) to ensure the safety. In the experiment, the controller of the robot was activated when the robot was bending down, and we then pushed the switch so as to supply the air to the Muscle Suit. HRP-4 was then lifted by the device, while the robot tracked the trajectory of the retargeted human motion.

The snapshots of the generated robot motion, as well as the original human motion, are shown at the lower row of Fig. 4.4. As can be seen, the robot could lift the upper trunk successfully while keeping the original appearance of the human motion. We also checked whether the actuator torque of the waist joint decreases by benefiting from the assistive effect. Figure 4.3 shows the actuator torque of the waist joint and the transition of the trajectory parameter x . The device switch was pushed at around 3 s, then the robot started the movement at 4 s, and finished the movement at around 11 s. From 3-4 s, the robot kept the starting bent posture because the assistive torque from the device was insufficient to lift the robot's trunk. Then, the absolute value of the actuator torque was within 10 Nm during 6-

11 s. Therefore, the proposed control framework successfully reduced the actuator torque of the robot while lifting its upper trunk. In contrast, the torque remained at about 20 Nm after stopping the motion. At the end of the motion, the velocity of the waist joint in the original human motion was equal to zero. It follows that $\frac{\partial \theta_{waist}}{\partial x}$, as well as the SR inverse in Equation (4.12) is usually equal to zero. When the velocity of trajectory parameter was almost equal to zero, our controller stopped the update of trajectory parameter. Though such a singularity happened at the end of the motion in our experiment, this issue will be addressed in future work.

4.4 Conclusion and Discussion

In this chapter, we introduced a humanoid controller for use of active wearable assistive devices by using path tracking. We focused on the human use of wearable assistive devices and considered two assumptions: first, human motion is constrained by the device worn; second, human motion involves minimal exertion as it fully exploits the assistive force. Based on those assumptions, we devised a new control scheme to track the retargeted human motion trajectory according to the supportive torque generated by the device.

The proposed method was applied to a pneumatically actuated wearable device called a “Muscle Suit”, which was strapped to the humanoid HRP-4. We have shown that the humanoid can track the given path, in accordance with the external force generated by the device, and that the proposed controller enables the human motion reproduction when using the wearable assistive device.

We have shown that the supportive effect of powerful active devices can be quantitatively evaluated during motion by using a humanoid robot. We are also well aware of several limitations to our approach.

First, variations in users’ size, alignment or motions should be addressed in any future work. This work was based on one subject’s measured motions, it will be important to analyze variance in several aspects over different subjects by measuring not only human but also the device. The motion model can be enhanced



Figure 4.4: Original human motion and retargeted humanoid motion. In human motion measurement, a human subject used the exhalation switch to activate the assistive device (Muscle Suit), and then lifted a 5-kg weight. The device provided the supportive force while switch is turned on. In the humanoid robot experiment, two 2-kg weights were attached to each wrist joint, and the device was activated by a switch controlled by an experiment operator. The robot started the lifting motion when the device was activated and provided enough supportive torque.

by taking into account those variances.

The second issue relates to the controller. The key contribution of proposed method is enabling evaluation of assistive torque during motion. However, this is a simplified method that leaves much room for improvement. Although we have measured human motions under assistance to be as close to actual use, we need to

go beyond the trajectory-tracking based controller to realize the motion sequence including motion without the device. The extended method is addressed in next chapter.

Chapter 5

Humanoid Controller for Motion Reproduction including Force Intervention

5.1 Introduction

The motion strategy of human might be changed during the motion sequence. In Chapter 4, the controller can only deal with the case of lifting-up motion. To achieve the motion reproduction including strategy changes, we introduce the path tracking controller using different strategies in this section.

In Chapter 4, we introduced the tracking control by using torque feedback. In that paper, we introduced a low-dimensional model as a reference of interaction between a robot and a device and realized human motion reproduction by a humanoid. However, the control scheme assumes that the low-dimensional model requires the one-to-one correspondence between the trajectory and the whole-body posture, so that the same body posture cannot be repeated in the same motion trajectory. Therefore, the previous control scheme cannot apply to the motion repeating the same postures like circle motions.

In this chapter, we propose a new control scheme that solves the above issue and allows the controller to reproduce the complex motion. In the proposed control

scheme, the two components are introduced: the external torque observer that estimates the assistive torque from an assistive device, and the tracking controller that reproduces human motion while achieving the desired interaction between a robot and a device based on the estimated external force. The combination of the two components finally generates the human-like whole-body movement of the robot according to the assistive forces applied by the device. We have conducted the experiments to validate the proposed control scheme by humanoid HRP-4 [57] with wearable assistive device Muscle Suit [31]. We also check whether the proposed method can extract the assistive effect of the device quantitatively.

This chapter is organized as follows: Section 5.2 presents the details of the new control system. Section 5.3 presents the experimental validation of the control scheme and the case study of testing the assistive effect by the proposed method.

5.2 Vector Field based Tracking Controller

We present the control framework for tracking a trajectory with interacting an active assistive device, considering following assumptions of the human behavioral intention when using the assistive device. The assistive device is often designed for the human body to support a typical task such as lifting an object. As a result, human motion is likely to follow an identical trajectory due to a geometric constraint of the mechanical structure of the device. Most devices can generate high assistive force to reduce human muscle effort. We assume that human muscles exert less forces when utilizing the device at assisted parts of human body. In fact, we have shown that the muscle effort when assisted by the device is similar to when it is relaxed, through the EMG signals analysis on the human subject experiment in Chapter 2.

Achieving that a humanoid reproduces human motion when using an assistive device, the humanoid has to track the human motion trajectory in response to the external force applied by the device. We show an overview of our control framework in Figure 5.1. The controller comprises two components; the torque observer that estimates an assistive torque and the tracking controller that achieves motion

reproduction with desired interaction. Combining these components, the tracking controller can compute the desired joint angles of the robot under consideration of the external torque to avoid the torque confliction between the robot and the device. With this controller, we can realize human motion reproduction on the humanoid robot in a similar interaction situation to that of humans. To create the target trajectory, we captured the human motion with a device and generate the feasible trajectory for humanoid by using the motion retargeting technology [18]. Based on our previous controller [59], we introduce the single phase parameter x that represents all the joint angle trajectories $\boldsymbol{\theta}$ of a robot when the robot tracks the trajectory.

$$\tau_{joint} + \tau_{ast} = f(x) \triangleq h(\boldsymbol{\theta}(x), \dot{\boldsymbol{\theta}}(x), \ddot{\boldsymbol{\theta}}(x)), \quad (5.1)$$

where τ_{joint} and τ_{ast} are the joint torque and external torque applied by an assistive device, respectively, and $f(x)$ or $h(\boldsymbol{\theta}(x), \dot{\boldsymbol{\theta}}(x), \ddot{\boldsymbol{\theta}}(x))$ is the torque coming from the inertial, Coriolis, and gravity forces.

The trajectories $\theta_{(x)}$ and the derivatives are designed according to the measured data of human motion by motion retargeting technology. In this study, we use the efficient motion retargeting method proposed in [18]. Here, we briefly explain the features of this method. Considering the differences of the body structures between the robot and humans, the method solves a simultaneous optimization problem, including the following three sub-problems:

1. Inverse kinematics problem that calculates the joint angle trajectories of a human model to achieve the measured motion.
2. Problem of identifying the morphing function between the human and robot models.
3. Motion-planning problem that considers physical consistency of the robot such as a balance or joint limits.

The humanoid motion is obtained as a result of the above optimization problem. Since the method involves the motion-planning problem, that trajectory of a humanoid can be achieved with no additional controllers. The method shown in [18]

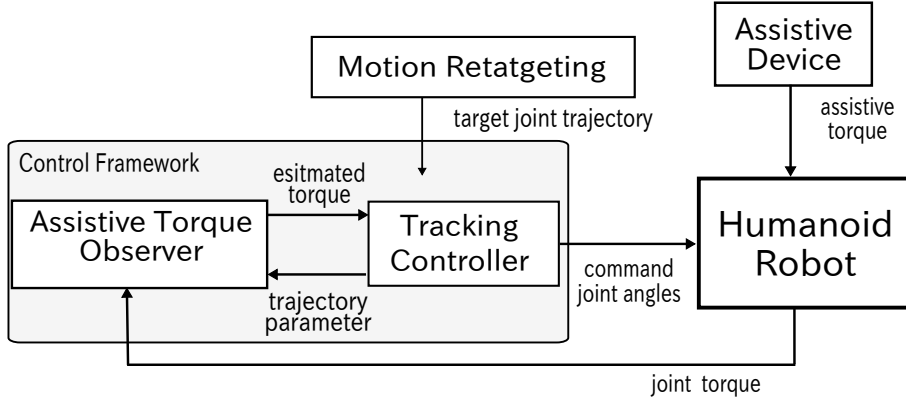


Figure 5.1: Overview of our controller

can also realize the inverse motion retargeting from humanoid to human, which can estimate the human motion reflecting the modification happened in the forward motion retargeting. Though the direct comparison between the dynamics of the human and that of the robot is difficult, the reproducibility about the motion retargeting can be quantified by comparing the difference between the original human motion and the estimated human motion. The detail of the evaluation is shown in [18].

We first present the external torque observer in Section 5.2.1. Then, we present the tracking control scheme in 5.2.2.

5.2.1 External Torque Observer

Figure 5.1 shows the summary of our controller. First, the external torque observer is presented for the estimation of the assistive torque. The tracking controller adjust x by using the estimated torque in order to achieve the desired interaction. In this study, we utilize the momentum based disturbance observer detailed in [60, 61]. The dynamics can be written as a transfer function when adding the residual value r .

$$\frac{r}{\tau_{joint}} = \frac{K}{s + K}, \quad (5.2)$$

where s is a Laplacian operator, K is observer gain ($K > 0$) and τ_{joint} is a joint torque in Equation (5.1). We can formulate the first order differential equation of r from Equation (5.2):

$$\dot{r} = -Kr + K\tau_{joint}, \quad (5.3)$$

Since the assistive torque cannot be measured directly, we observe the residual value r as $f_{(x)} - \tau_{ast}$ in Equation (5.1). Replacing r with $f_{(x)} - \tau_{ast}$, Equation (5.3) can be written via τ_{ast}

$$\dot{\tau}_{ast} = -K\tau_{ast} + K(f_{(x)} + \tau_{joint}) - \dot{f}_{(x)}, \quad (5.4)$$

From above equation, we can track the evolution of the external torque τ_{ast} during the motion. Practically, we discretize Equation (5.3) and reformulate as:

$$\begin{aligned} \hat{\tau}_{ast}[t+1] &= (1 - K\Delta t)\hat{\tau}_{ast}[t] \\ &+ K\Delta t(f_{(x[t])} + \tau_{joint}) - \dot{f}_{(x[t])}, \end{aligned} \quad (5.5)$$

where $\hat{\tau}_{ast}$ is an estimated assistive torque and Δt is a time step of a controller. $\dot{f}_{(x)}$ is derivative of $f_{(x)}$, computed in the following controller:

5.2.2 Tracking Controller based on External Torque

The observer gives the assistive torque to the tracking controller. Then, the tracking controller adjusts the parameter x to achieve human motion reproduction. We call the space expressed in the parameter x and torque τ as x - τ interaction space and the state is written as (x, τ) . Adjusting x in response to the estimated torque $\hat{\tau}_{ast}$, we designed an interaction model in $x - \tau$ space. According to our assumption, the desired interaction is achieved when the assisted joint torque is equal to be zero ($\tau_{joint} = 0$), which is equivalent to $\tau_{ast} = f_{(x)}$. We computed the reference torque trajectory $f_{(x)}^{trg}$ that is required to realize the given motion without using an assistive device. Therefore, the controller computes desired x (x^{des}) in such a way as to satisfy $\hat{\tau}_{ast} = f_{(x)}^{trg}$. However, when the multiple values of x^{des} satisfying $\hat{\tau}_{ast} = f_{(x)}^{trg}$ exist, the controller cannot compute unique x^{des} , which is the case that

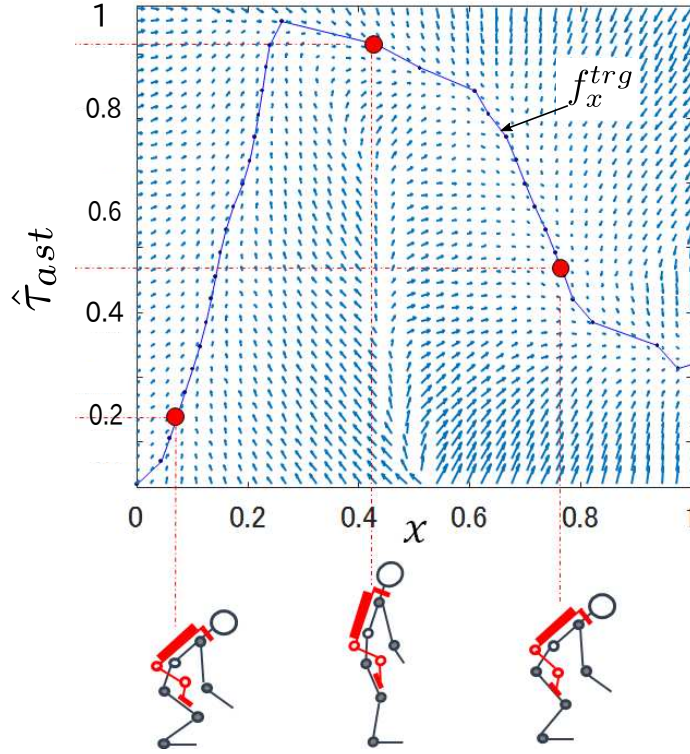


Figure 5.2: Relationship between the desired state $(x, f(x))$ in the interaction model and a current robot state $(x, \hat{\tau}_{ast})$ with the vector field. The solid line is the target trajectory $f_{(x)}^{trg}$ generated by the motion retargeting method and the arrows denote the gradient vectors at each point in the space.

trajectory does not have the one-to-one correspondence between x and $f(x)$. In these cases, the computation of x is indeterministic due to the singularity, and causes the instability of the controller. To solve this problem, we design the vector field to attract current x to the nearest x^{des} so that the controller can achieve the nearest x^{des} .

We introduce the tracking control based on a vector field in x - τ space as shown in Figure 5.2. Figure 5.2 shows an example of the reference torque trajectory (blue solid line) when a humanoid reproduces the lif-up motion with an assistive device; a vertical axis denotes normalized $\hat{\tau}_{ast}$ and a lateral axis denotes normalized x corresponding to a humanoid posture. The vector field is designed to attract the

current state of $(x, \hat{\tau}_{ast})$ to the desired state $(x^{des}, \hat{\tau}_{ast} = f^{trg}(x^{des}))$ by giving a velocity of x . Therefore, the vector field is represented below function:

$$\dot{x} = V(x, \hat{\tau}_{ast}). \quad (5.6)$$

Here, we can also compute $\dot{\hat{\tau}}_{ast}$ in same as \dot{x} . $\dot{\hat{\tau}}_{ast}$ is a change of the torque due to a change of x . Therefore, we assume $\dot{\hat{\tau}}_{ast} = \dot{f}_{(x)}$ while $\tau_{joint} \simeq 0$ in Equation (5.1) and we utilize $\dot{\hat{\tau}}_{ast}$ as $\dot{f}_{(x)}$ in Equation (5.4).

The procedure of the vector field creation is follows: The reference trajectory $\mathbf{f}_{(x)}^{trg}$ can be computed by inverse dynamics computation using target trajectory $(\theta(x), \dot{\theta}(x), \ddot{\theta}(x))$ generated by motion trajectory method. $\mathbf{f}_{(x)}^{trg}$ is given as a sequence data including n size data set ($\mathbf{f}_{(x)}^{trg} = [f_{(x[1])}^{trg}, f_{(x[2])}^{trg}, \dots, f_{(x[i])}^{trg}, \dots, f_{(x[n])}^{trg}]$). Now, we assume a target trajectory as \mathbf{a} :

$$\mathbf{a} = [\mathbf{a}_1, \dots, \mathbf{a}_i, \dots, \mathbf{a}_n] \quad (5.7)$$

$$= [(x[1], f_{(x[1])}^{trg}), \dots, (x[i], f_{(x[i])}^{trg}), \dots, (x[n], f_{(x[n])}^{trg})]. \quad (5.8)$$

then, a vector $V_c(x, \hat{\tau}_{ast})$ at a point \mathbf{c} is determined by following procedure:

1. find the closest point $\mathbf{a}_i(x[i], f_{x[i]}^{trg})$, from a point \mathbf{c} in \mathbf{a} as shown in Figure 5.3;
2. compute a vector from a current point \mathbf{c} to \mathbf{a}_i that pulls in the trajectory, and a vector from \mathbf{a}_i to \mathbf{a}_{i+1} that is a flow to the next state;
3. compose two vectors and compute $V_c(x, \hat{\tau}_{ast})$ by

$$V_C(x, \hat{\tau}_{ast}) = K_v(a_i - c) + K_v(a_{i+1} - a_i). \quad (5.9)$$

Applying the above procedure over all points in the space, the vector field can be obtained as shown in Figure 5.2. From the vector field, $\dot{x}[t+1]$ is given by the vector $V(x[t], \hat{\tau}_{ast})$ at each control period t :

$$\dot{x}[t+1] = V(x[t], \hat{\tau}_{ast}[t]) \quad (5.10)$$

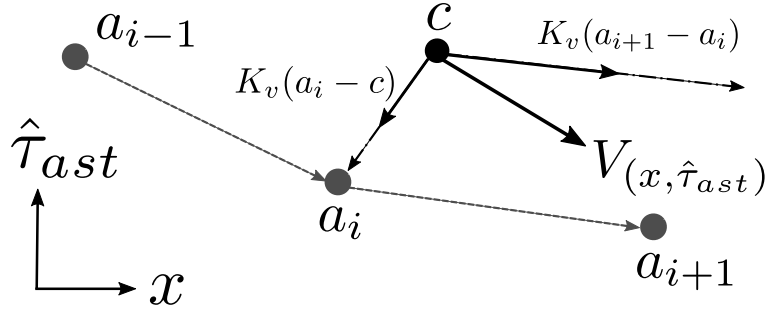


Figure 5.3: Defining the vector at the point $C(x, \hat{\tau}_{ast})$. $x, \hat{\tau}_{ast}$ are current state, $f_{(x[i])}^{trg}$ is the closest point of trajectory from C , $i = 1, 2, \dots, n$.

The above control framework realizes that a humanoid robot tracks the human motion trajectory while its joint is fully supported by the assistive device. The following section provides an experimental validation of our controller and an evaluation of the assistive device by using the controller.

5.3 Experiments on Humanoid

We tested the proposed controller with a human-sized humanoid robot and a commercialized assistive device Muscle Suit. We first validate whether the controller can be applied to the motion trajectory. we chose to lift an object up and down motion as a typical task when using the assistive device for supporting lower back. It is also checked whether the assistive torque of the device can be extracted quantitatively by using our controller through our evaluation framework.

5.3.1 Experimental Setup

The experiments were conducted with humanoid HRP-4 [57], the Muscle Suit [27, 48] that are explained previous Section 4.3.1.

We captured the human motion which represents the target trajectory in our control framework. In the measurement experiment, we used the motion capture system (Motion Analysis) and recorded the motion trajectory of a human subject

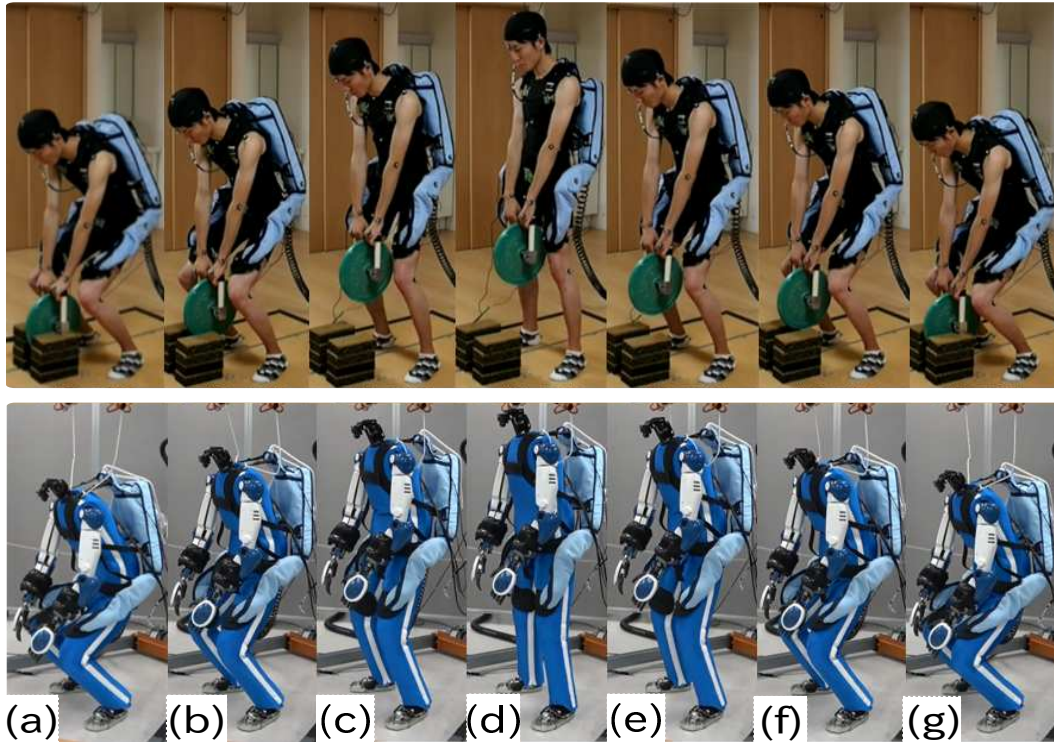


Figure 5.4: Result of human motion reproduction by the proposed controller. When the assistive device is activated (starts supporting), the robot starts lift-up motion ((a)-(c)). After achieving an upright posture (d), the robot keeps the posture until the device is deactivated. Finally, the robot put the weight down while the supportive effect decreases ((e)-(g)).

lifting a 5 kg weight; the subject wearing Muscle Suit bends down to catch the weight, lifts it up, and puts it down. The recorded motion was retargeted to the feasible trajectory of the humanoid robot by using the motion retargeting method detailed in [18]. The vector field used in the controller was generated from the retargeted trajectory by using the creation procedure mentioned in 5.2.2. Since the retargeted trajectory is generated with taking into account the joint limits or balancing, the robot can reproduce the motion without extra controllers.

5.3.2 Experimental Validation of Proposed Controller

We tested our controller on HRP-4 with the Muscle Suit by using the proposed controller. In this experiment, we attached the 4-kg weight to the wrist joints of the robot (2 kg to each wrist) in advance to avoid executing the object grasping task. The robot postures reproduced by the proposed controller are shown in Figure 5.4. The humanoid was first crouched with its waist bending (posture (a)), and then the robot started lift-up motion (posture(b-c))when the device was activated and starts supporting the waist joint. After the lifting-up motion was over (posture (d)), the robot kept an upright posture while its waist joint get supported by the device. Finally, the robot bent down after we deactivated the device (posture (e-g)). The robot can replicate the entire sequence of up/down motion, as seen from the snapshots. It should be noted that the controller does not know the timing when the human operator activated or deactivated the device. In accordance with the interaction model of the robot device developed by the tracking control, the robot automatically started lifting or putting down.

In the upper ranges of Figure 5.5, the result of the torque assessment is shown. In this experiment, we assumed that the assistive torque is equivalent to the desired torque ($\hat{\tau}_{ast}(t = 0) = f_{(x(0))}$) when the observer was initialized ($t = 0$). This assumption is necessary, since the robot already has a weight in front of the device. In actual human use, we can presume that the human beginning is sufficiently supported when the lower back is lifted. This conclusion is thus known as the observer's offset. As a result, the activation timing of the tracking controller was adjusted to a timing when the joint torque in upper row of was zero at about 3.5 s (Figure 5.5). The assisted torque can be estimated during the robot reproducing a movement.

While the observer estimates the assistive torque, the tracking controller adjusts x , so that the estimated torque $\hat{\tau}_{ast}$ can track the desired torque $f^{trg}(x)$. The result of adjusting x is shown in the lower row of Figure 5.5. From the vector field based tracking controller, \dot{x} as the velocity of x was determined. Then, x gave whole-body joint angles, and the robot reproduced the posture that satisfied $\hat{\tau}_{ast} = f_{(x)}^{trg}$.

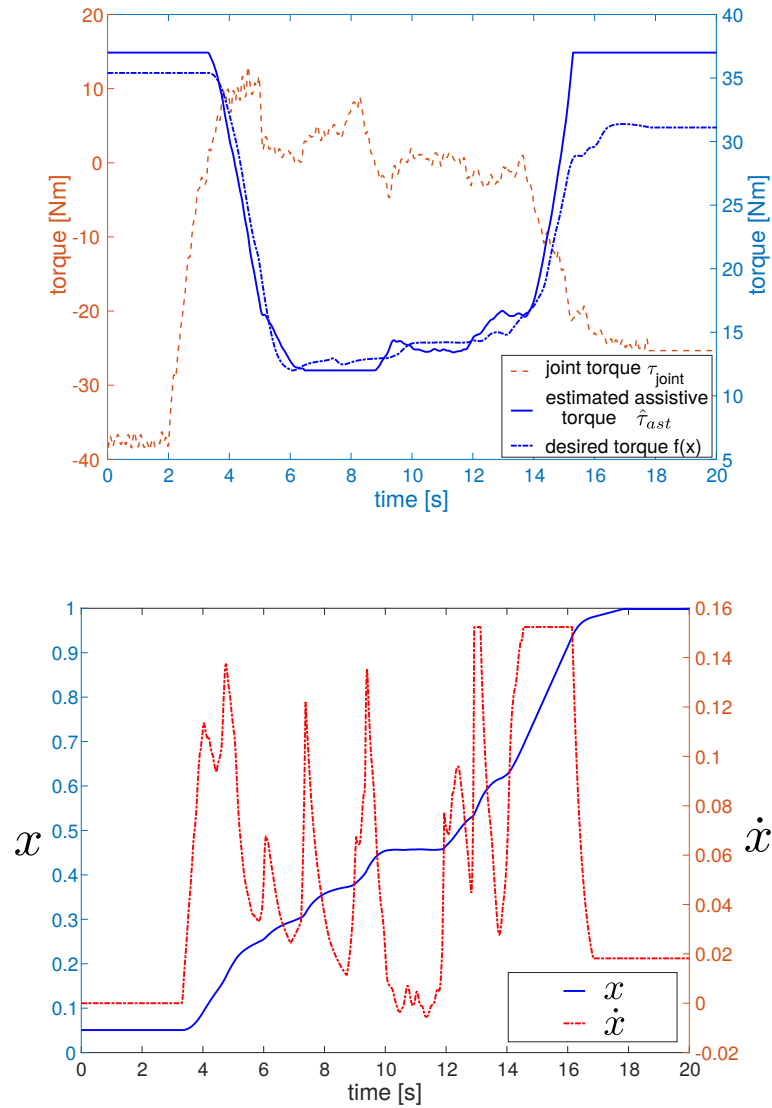


Figure 5.5: Result of assistive torque observer (upper row) and tracking controller (lower row).

As a result, $\hat{\tau}_{ast}$ tracks $f_{(x)}^{trg}$ in Figure 5.5. Since the robot movement was ended around 17.0 s, the tracking error $f_{(x)}^{trg} - \hat{\tau}_{ast}$ became bigger.

5.4 Conclusion and Discussion

In this chapter, we proposed a control framework for realizing human motion reproduction when wearing the assistive device (exoskeleton) and moving cooperatively with it. The proposed control framework comprises the two different components: (A) the assistive torque observer using the momentum based disturbance observer. (B) The tracking controller based on the vector field designed according to the robot/device interaction model. Combining two components, the robot can imitate the actual usage situation when human muscles are relaxed during the movement when wearing the device. Since our control framework was developed for evaluating the general assistive device, the framework is independent of the device controller so that the robot can achieve the motion reproduction with no modification of the device. Therefore, the robot can wear the device in the same way as humans do and test it. In addition, the proposed framework can evaluate the assistive device by quantifying the assistive effect from the sensor values of the robot. The device evaluation by using the proposed method is to be addressed in Section 6.

To validate our control framework, the human motion was recorded by the motion capture system in advance. We recorded the continuous sequence of motion when lifting up and down an object with wearing the device. The recorded motion was used to design the vector field of the controller (B). Then, the proposed control framework was tested by using humanoid HRP-4 wearing the assistive device Muscle Suit. The results of the experiment clearly showed that the robot could move cooperatively while the device assists the waist joint in the same way as humans do. Thanks to the controller (B), we could also generate the continuous sequence of the lifting operation, even though the robot does not know the control state of the assistive device.

In this study, the controller vector field (B) was simply designed from the retargeted human motion. The vector field can represent several characteristics of human motion control. For example, the variance in motion trajectories performing the same tasks depends on how the trajectory in the vector field is pulled in [62, 63].

For more accurate and natural use situations, the advanced design of the vector field is important and will be investigated in the future.

Chapter 6

Assistive Device Evaluation with Humanoid Robot

In this chapter, our evaluation of an active assistive device with the proposed method is presented.

6.1 Experimental Setup

The experiment was conducted with the humanoid robot “HRP-4” and Muscle Suit, which is mentioned above. The proposed framework requires that the humanoid robot have a geometric structure similar to that of a human. HRP-4 is among the most suitable robots for this experiment because its geometric structure is designed according to anthropometric data of average young Japanese females. For discussing the differences in the kinematic properties of human users and humanoid HRP-4, we compare the weight of each body link from the robot model data and the human body segment inertial parameters reported by Dumas et al. [64]. The ratio of the weight of each body link of HRP-4 is calculated and compared with the data of females from the Dumas database, as shown in Table 6.1. From Table 6.1, although the ratio of each body link of HRP-4 is not similar to that of humans, the ratio of the entire upper and lower body is similar to that of humans. The robot used herein has 37 degrees of freedom (each arm: 9, each leg: 7 includ-

Table 6.1: Comparison of mass properties between human and HRP-4

| Body link | HRP-4 (%) | Human (%) |
|--------------------|-----------|-----------|
| HEAD | 1.6 | 6.7 |
| ARM | 9.8 | 4.0 |
| TORSO | 20.0 | 30.4 |
| Upper body (total) | 41.2 | 45.1 |
| WAIST | 17.7 | 14.6 |
| LEG | 20.5 | 20.1 |
| Lower body (total) | 58.7 | 54.8 |

ing one at the toe, chest: 3, neck: 2), which means it can reproduce human-like motions. Because our focus is the waist joint, which Muscle Suit mainly supports, the robot provides reliable torque measurements of the kinematic properties of the entire trunk.

Though the standard HRP-4 robot is fitted with a hard cover, we replaced it with a soft fabric to which several types of wearable devices can be attached. In Figure 4.2, we show HRP-4 wearing Muscle Suit; no additional attachment is required, and the device can be installed on the robot as it can be on humans. The weight to be lifted is attached near the chest joint of the robot.

6.2 Evaluation Framework for Wearable Assistive Device

In Chapter 4 and 5, we showed that our controller allows humanoid to reproduce the human motion when wearing the device. In this chapter, with the proposed controller, we evaluated the assistive device Muscle Suit by the following procedures (Figure 6.1):

1. The humanoid robot wearing the device reproduces a human motion by using the proposed controller. During the motion, we recorded both the joint angles and torques of the robot.

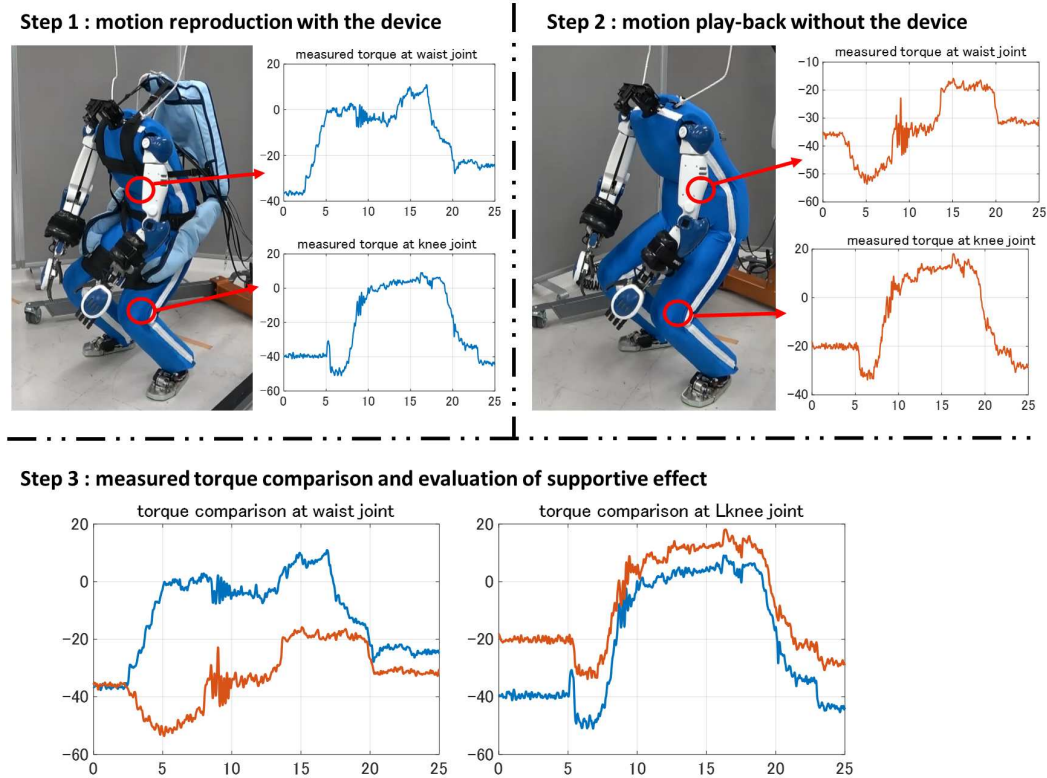


Figure 6.1: Procedure of the assistive torque extraction; step 1) measuring the joint torques with the device by using the proposed controller; step 2) measuring the joint torques without the device by playing-back the motion recorded in step 1; step 3) comparing the joint torques measured with device and without device.

2. The humanoid robot play-back the same motion as that recorded in 1) without the device. The joint torques were recorded during the movement.
3. The motion performed in step 1) and step 2) are same geometric trajectory while the robot uses the device in step 1) but the robot doesn't use it in step 2). By comparing the difference of the torques measured in 1) and 2), the assistive torque of the device during the movement could be extracted quantitatively.

We conducted the evaluation with different weight condition; 4-kg weight and 6-kg weight. The experimental conditions are summarized in Table. 6.2 for step

Table 6.2: Experimental condition in step 1) and 2)

| | step 1) | step 2) |
|---------------|-----------------------|------------------|
| weight | 4kg, 6kg | 4kg, 6kg |
| device | use | not use |
| measured data | joint angles, torques | joint toques |
| controller | proposed controller | servo controller |

1) and 2) respectively. The joint torque comparison between the motion with the device and without the device are shown in Figure 6.2 and 6.3 for each case of 4-kg and 6-kg, respectively. In both results, the red solid line shows the torque when using the device and the blue line indicates that without the device. The bending direction generates the positive value of the torque and the straightening direction generates the negative one. In figures, the motion sequences are divided by 3 periods; first period is weight lifting-up motion corresponding to the robot posture depicted in (a) to (c) in Figure 5.4, second period is weight keeping motion corresponding to the posture depicted in (d) in Figure 5.4, last period is weight putting-down motion corresponding to the posture depicted in (e)-(g) in Figure 5.4.

With the 4-kg weight in Figure 6.2, the motion continued for about 15 s; the robot lifts a weight in 6-12 s, then keep it with its up straight posture in 12-18 s, and finally puts it down in 18-21 s. That continued for about 17 s with 6-kg weight in Figure 6.3. These results show that our controller appropriately adjust x so that the robot can reproduce the motion in the different conditions.

In both results, the torque with the device is decreasing when the robot moves, and converges, which denotes the proposed controller successfully realized the motion with the benefit of assistive torque instead of using the robot joint torque. Without the assistive device, high torque is required to execute the same motion. According to both results, the peak torques (around 65 Nm at 8 s in 4-kg case and around 80 Nm at 5 s in 6-kg case respectively) were efficiently reduced when the

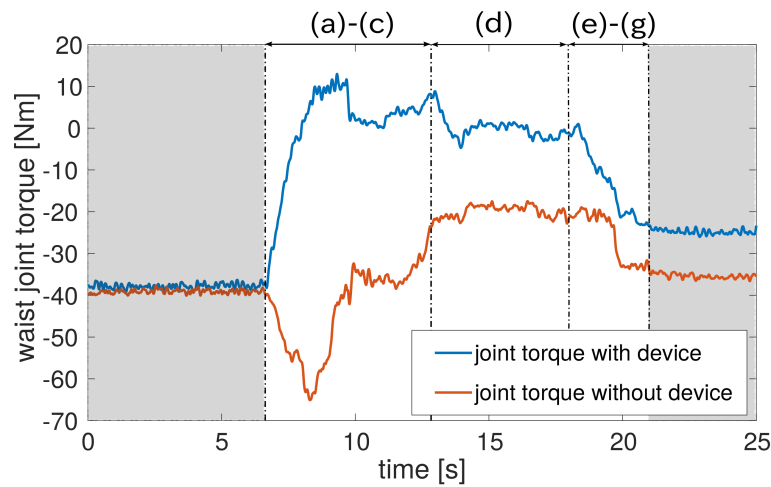


Figure 6.2: Torque comparison of the lift-up 4kg weight motion with the device and without device. The motion starts around 6 s when the joint torque changes. The motion continued for 15 s until it ended around 21 s. The motion is divided by 3 periods; first period (6-13 s) is corresponding to motion depicted in (a) to (c) in Figure 5.4, second period (13-18 s) is corresponding to motion depicted in (d) in Figure 5.4, last period (18-21 s) is corresponding to motion depicted in (e) to (g) in Figure 5.4.

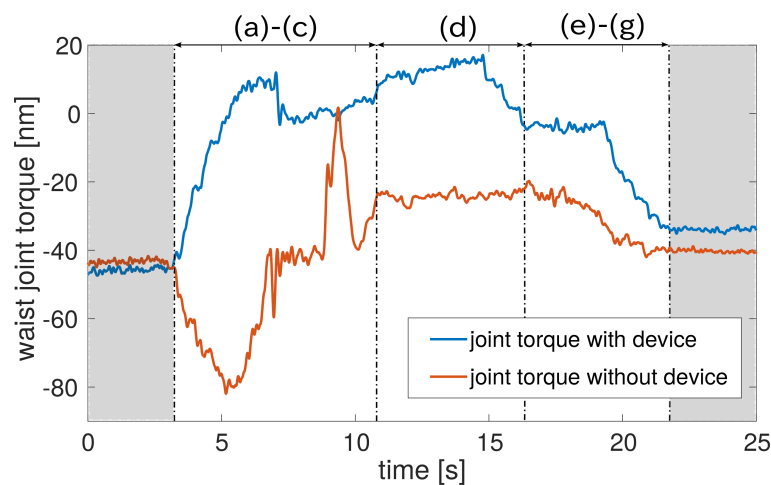


Figure 6.3: Torque comparison of the lift-up 6kg weight motion with the device and without device. The motion starts around 4 s when the joint torque start changes. The motion continued for 17 s until it ended around 22 s.

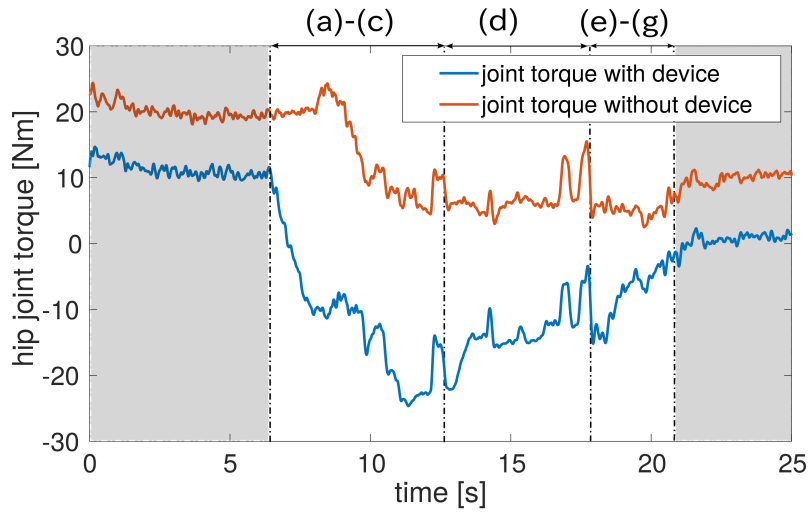


Figure 6.4: Hip joint torque comparison of the lift-up 4kg weight motion with the device and without device.

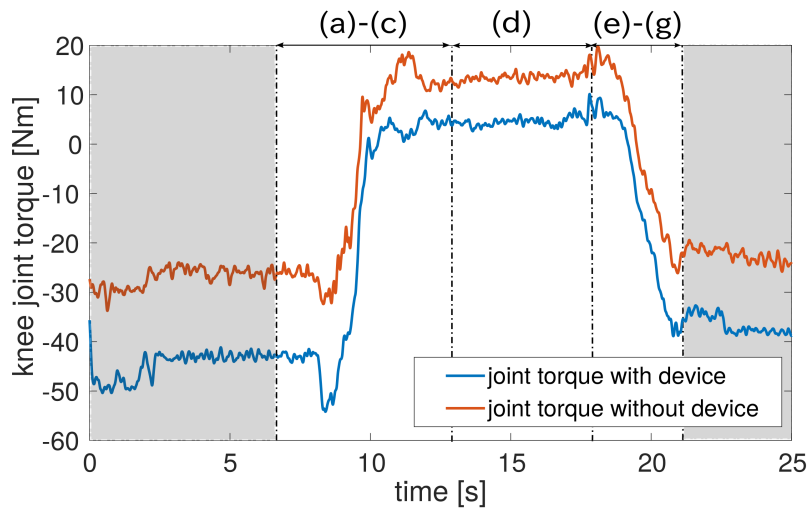


Figure 6.5: Knee joint torque comparison of the lift-up 4kg weight motion with the device and without device.

robot wearing the device. As seen in both figures, the device reduced the waist joint torque through the overall motion.

Since the Muscle Suit mainly supports the waist joint, we focus on the supportive effect at the waist joint. To confirm the effect of the device at other joints,

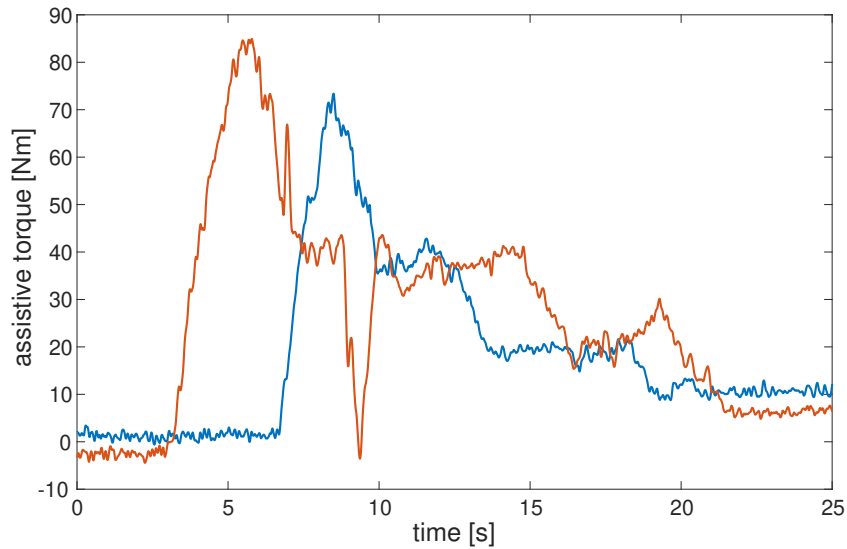


Figure 6.6: Result of the assistive torque extraction. The blue line denotes the assistive torque with 4-kg weight and the red one denotes that with 6-kg weight

torque changes of other joints were also compared. The hip joint torque comparison is shown in Figure 6.4. Since the device covers the hip joints of the robot, the hip joint gets affected by the supportive effect. The hip joint torque is reduced by using the device in the period when the robot was not moving highlighted by gray in Figure 6.4. The torque increases by using the device in the period when the robot is moving. This increase in the hip joint torque was caused by reaction to the reduction of the waist joint torque. However, the increase torque of the hip joint is sufficiently small compared to the decrease torque of the waist joint. The knee joint torque comparison is also shown in Figure 6.5. The knee joint does not get affected by the supportive effect because the device is attached to the body above the knee. Therefore, the increase in the knee joint torque is due to the increase in weight of the device.

Finally, the assistive effects of the device were extracted by subtracting the torque with the device from that without the device in each case respectively as

shown in Figure 6.8. The assistive torque with 4-kg weight is approximately 30 Nm on average during the motion and its peak value is 70 Nm which was observed when the robot started lifting up motion. With 6-kg weight, the average torque is around 40 Nm and the peak torque is 85 Nm which was also observed when the robot started motion. From this result, we successfully visualize the assistive effect of the device by using the humanoid.

6.3 Conclusion and Discussion

In this chapter, we proposed the evaluation framework of the wearable assistive devices. The proposed framework could extract the assistive torque generated by the device during the whole motion sequence. Since extracting the assistive torque of the device is difficult in the human subject experiments, the evaluation using the humanoid robot has a great benefit in providing the performance index to users. The proposed control scheme can perform without the specific model of the device, which shows that we can evaluate the other wearable assistive devices in the same manner.

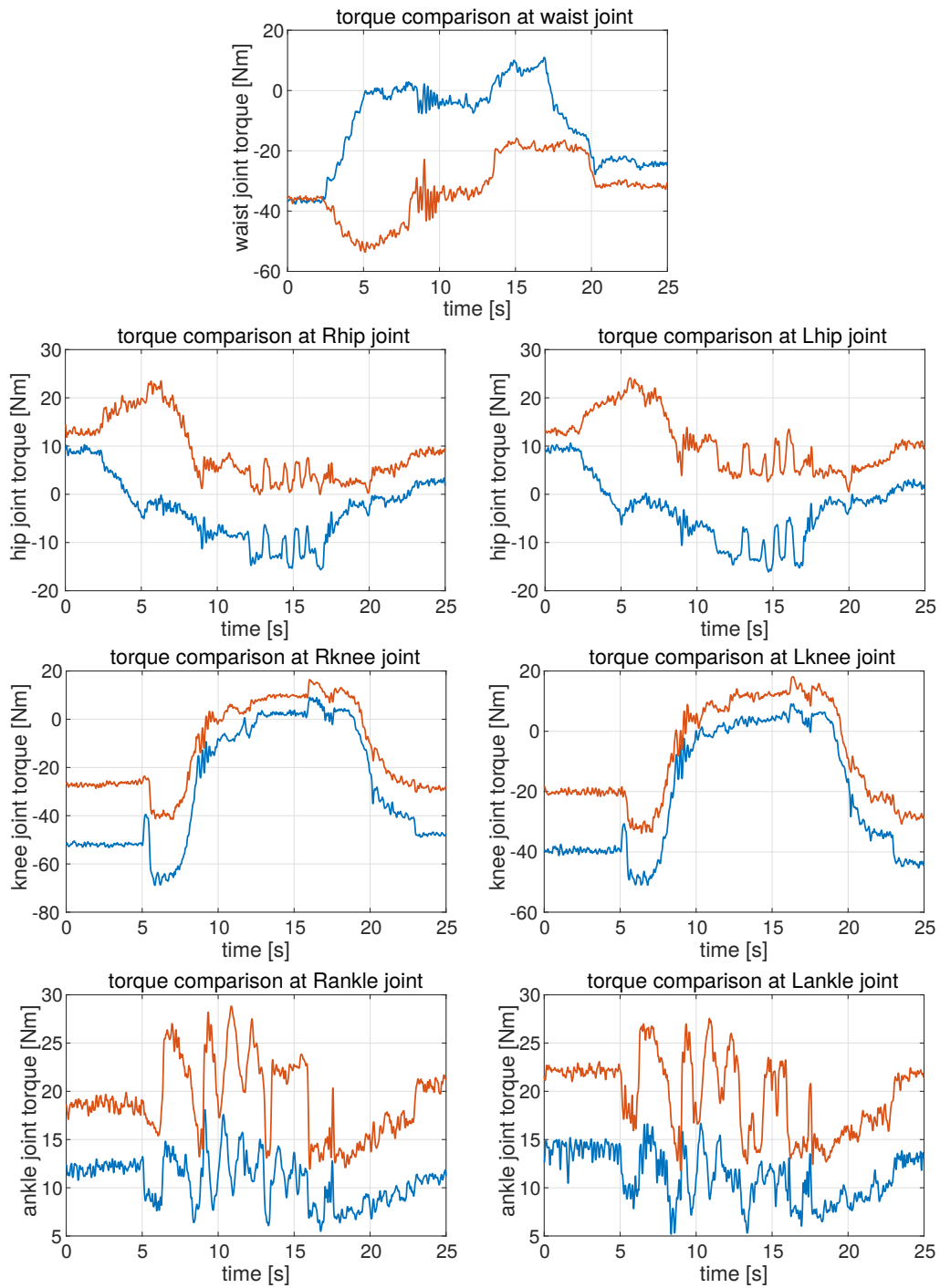


Figure 6.7: All joint torque comparison of the lift-up 4kg weight motion with the device and without device. In all results, the blue solid line shows the torque when using the device and the red line indicates that without the device.

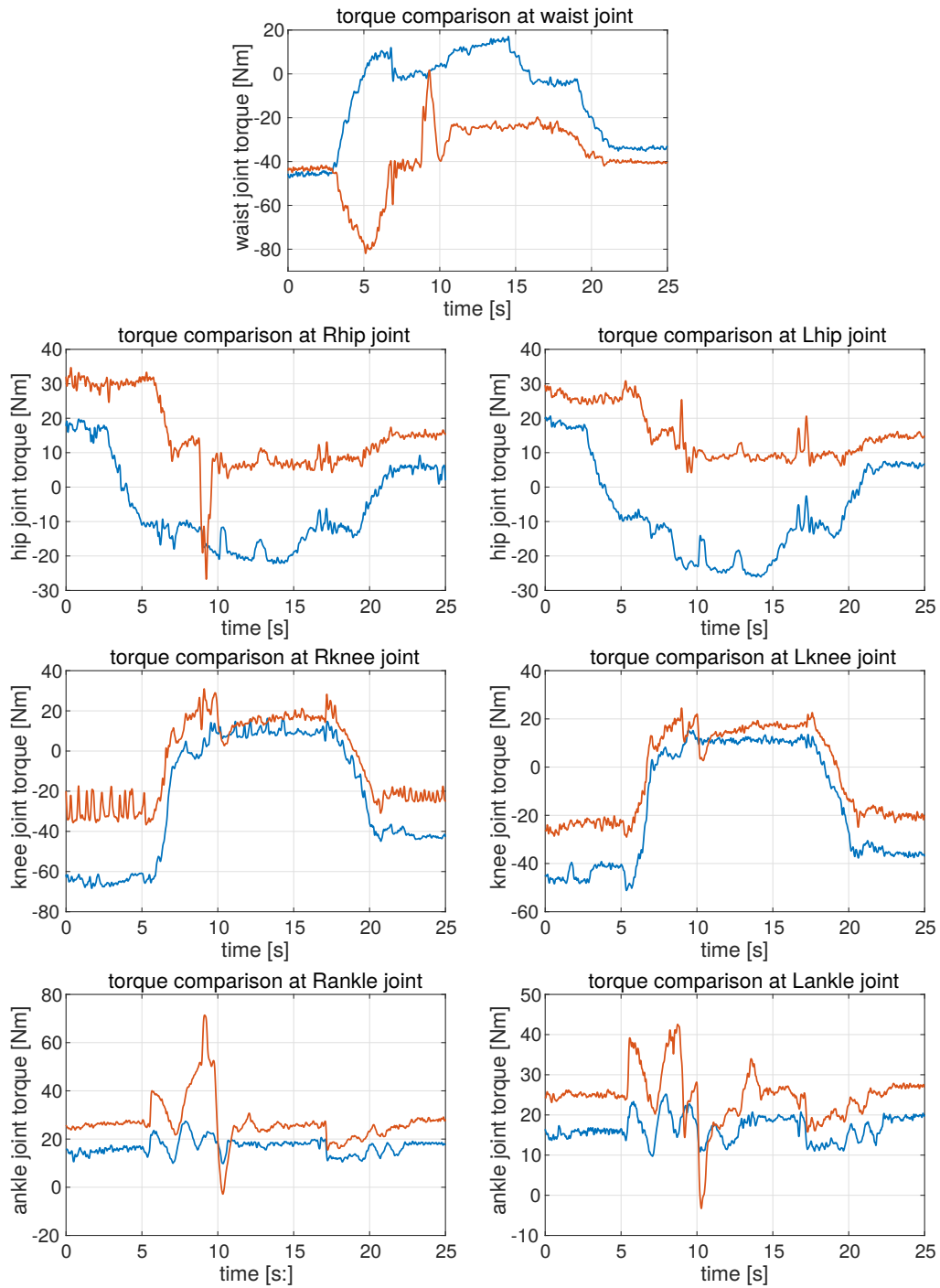


Figure 6.8: All joint torque comparison of the lift-up 6kg weight motion with the device and without device. In all results, the blue solid line shows the torque when using the device and the red line indicates that without the device.

Chapter 7

Conclusion

In this thesis, we studied the human motion using the force intervention, that is, the external forces exertion that contribute to achieve the motion. We have focused on the motion using wearable assistive devices as a typical example that humans utilize the force intervention. From the result of the human motion analysis, human motion strategy utilizing the force intervention was extracted. Then assuming that strategy, the humanoid controller to realize the human motion reproduction could be achieved. We have also outlined the use of humanoid robots as the human body simulator, which provides the quantitative measurement of the internal forces.

The major contribution of this thesis is that we analyzed the human motion when utilizing the force intervention, the external force exertion by the assistive device. In addition to using the general method of the human internal forces estimation based on the inverse dynamics computation, we introduced the analysis of the human muscular activity based on EMG measurement and observed the human internal forces and the external forces applied by the device, respectively. Although the result of this study was limited in the experiments under using the particular device, we believe our method could be applied to the various devices.

In this thesis, we also introduced the humanoid controller for the human motion reproduction including physical interaction with the device. The proposed controller was developed by considering the human motion strategy of the interaction with a device so that the robot can replicate the motion in similar manner

to that of humans. The proposed controller enabled the humanoid robot to be used as the human body simulator, and provided the quantitative measurement of the assistive torque applied by the device. Therefore, our evaluation method using the humanoid robot has a great benefit in providing the performance index of the device to users who select the suitable device from many devices.

The summaries of the studies presented in this thesis are follows.

- (i). The human subject experiments were conducted to observe the force intervention applied by the wearable assistive device during the motion. To observe the external forces during experiments, The method based on the inverse dynamics computation and muscular activities measurement was introduced to distinguish the external forces from the internal forces on human body. By using the method and analyzing the motion, the assumptions of the human motion strategy when utilizing the force intervention were extracted. For humanoid robot to observe the force intervention, the contact estimator for the robot was also introduced.
- (ii). Based on the human motion strategy assumed in (i), the humanoid controller that can imitate the use of the force intervention was presented. The proposed controller was developed using the torque-based trajectory tracking control so that the humanoid robot can reproduce the human motion trajectory. We applied these approaches to the case that human utilizes the force intervention by the wearable assistive device, and realized the motion reproduction with a real humanoid robot wearing the device.
- (iii). The evaluation framework for an active assistive devices was proposed. The extraction of the assistive effect of the device was achieved by our proposed framework, that is difficult in human subject experiments. Since our control framework was developed for evaluating the general assistive devices, the framework is independent of the device controller. Actually, the proposed control scheme can perform without the specific model of the device, which indicates that we can evaluate the other wearable assistive devices in the

same manner. so that the robot can achieve the motion reproduction without any modification of the device. By using the proposed framework, we could extract the assistive torque generated by the device during the whole motion sequence.

Bibliography

- [1] K. Kaneko, H. Kaminaga, T. Sakaguchi, S. Kajita, M. Morisawa, I. Kumagai, and F. Kanehiro, “Humanoid robot hrp-5p: An electrically actuated humanoid robot with high-power and wide-range joints,” *IEEE Robotics and Automation Letters*, vol. 4, no. 2, pp. 1431–1438, 2019.
- [2] G. Metta, G. Sandini, D. Vernon, L. Natale, and F. Nori, “The icub humanoid robot: an open platform for research in embodied cognition,” in *Proceedings of the 8th workshop on performance metrics for intelligent systems*, pp. 50–56, ACM, 2008.
- [3] T. Yoshiike, M. Kuroda, R. Ujino, H. Kaneko, H. Higuchi, S. Iwasaki, Y. Kanemoto, M. Asatani, and T. Koshiishi, “Development of experimental legged robot for inspection and disaster response in plants,” in *2017 IEEE/RSJ International Conference on Intelligent Robots and Systems (IROS)*, pp. 4869–4876, IEEE, 2017.
- [4] O. Stasse, T. Flayols, R. Budhiraja, K. Giraud-Esclasse, J. Carpentier, J. Mirabel, A. Del Prete, P. Souères, N. Mansard, F. Lamiraux, *et al.*, “Talos: A new humanoid research platform targeted for industrial applications,” in *2017 IEEE-RAS 17th International Conference on Humanoid Robotics (Humanoids)*, pp. 689–695, IEEE, 2017.
- [5] N. A. Radford, P. Strawser, K. Hambuchen, J. S. Mehling, W. K. Verdeyen, A. S. Donnan, J. Holley, J. Sanchez, V. Nguyen, L. Bridgwater, *et al.*,

-
- “Valkyrie: Nasa’s first bipedal humanoid robot,” *Journal of Field Robotics*, vol. 32, no. 3, pp. 397–419, 2015.
- [6] “Asimo : Honda motors co. inc..” <https://asimo.honda.com/default.aspx>, 11 2019.
- [7] Y. Sakagami, R. Watanabe, C. Aoyama, S. Matsunaga, N. Higaki, and K. Fujimura, “The intelligent asimo: System overview and integration,” in *IEEE/RSJ international conference on intelligent robots and systems*, vol. 3, pp. 2478–2483, IEEE, 2002.
- [8] “icub : Iit.” <http://www.icub.org/index.php>, 11 2019.
- [9] A. Schmitz, U. Pattacini, F. Nori, L. Natale, G. Metta, and G. Sandini, “Design, realization and sensorization of the dexterous icub hand,” in *2010 10th IEEE-RAS International Conference on Humanoid Robots*, pp. 186–191, IEEE, 2010.
- [10] “Atlas : Boston dynamics.” <https://www.bostondynamics.com/atlas>, 11 2019.
- [11] K. Kaneko, M. Morisawa, S. Kajita, S. Nakaoka, T. Sakaguchi, R. Cisneros, and F. Kanehiro, “Humanoid robot hrp-2kai –improvement of hrp-2 towards disaster response tasks,” in *2015 IEEE-RAS 15th International Conference on Humanoid Robots (Humanoids)*, pp. 132–139, IEEE, 2015.
- [12] K. Kaneko, F. Kanehiro, S. Kajita, H. Hirukawa, T. Kawasaki, M. Hirata, K. Akachi, and T. Isozumi, “Humanoid robot hrp-2,” in *2015 IEEE-RAS 15th International Conference on Humanoid Robots (Humanoids)*, pp. 132–139, IEEE, 2015.
- [13] Y. Ogura, H. Aikawa, K. Shimomura, H. Kondo, A. Morishima, H.-o. Lim, and A. Takanishi, “Development of a new humanoid robot wabian-2,” in *Proceedings 2006 IEEE International Conference on Robotics and Automation, 2006. ICRA 2006.*, pp. 76–81, IEEE, 2006.

-
- [14] A. M. M. Omer, H. Kondo, H.-o. Lim, and A. Takanishi, "Development of walking support system based on dynamic simulation," in *2008 IEEE International Conference on Robotics and Biomimetics*, pp. 137–142, IEEE, 2009.
- [15] G. Nelson, A. Saunders, N. Neville, B. Swilling, J. Bondaryk, D. Billings, C. Lee, R. Playter, and M. Raibert, "Petman: A humanoid robot for testing chemical protective clothing," *Journal of the Robotics Society of Japan*, vol. 30, no. 4, pp. 372–377, 2012.
- [16] K. Miura, E. Yoshida, Y. Kobayashi, Y. Endo, F. Kanehiro, K. Homma, I. Kajitani, Y. Matsumoto, and T. Tanaka, "Humanoid robot as an evaluator of assistive devices," in *Proc. 2013 IEEE Int Conf. Robotics and Automation*, pp. 671–677, 2013.
- [17] K. Ayusawa, E. Yoshida, Y. Imamura, and T. Tanaka, "New evaluation framework for human-assistive devices based on humanoid robotics," *Advanced Robotics*, vol. 30, no. 8, pp. 519–534, 2016.
- [18] K. Ayusawa and E. Yoshida, "Motion retargeting for humanoid robots based on simultaneous morphing parameter identification and motion optimization," *IEEE Transactions on Robotics*, vol. 33, no. 6, pp. 1343–1357, 2017.
- [19] K. Yamane and J. Hodgins, "Simultaneous tracking and balancing of humanoid robots for imitating human motion capture data," in *2009 IEEE/RSJ International Conference on Intelligent Robots and Systems*, pp. 2510–2517, IEEE, 2009.
- [20] W. Suleiman, E. Yoshida, F. Kanehiro, J.-P. Laumond, and A. Monin, "On human motion imitation by humanoid robot," in *2008 IEEE International Conference on Robotics and Automation*, pp. 2697–2704, IEEE, 2008.
- [21] J. Koenemann, F. Burget, and M. Bennewitz, "Real-time imitation of human whole-body motions by humanoids," in *2014 IEEE International Conference on Robotics and Automation (ICRA)*, pp. 2806–2812, IEEE, 2014.

-
- [22] Y. Sankai, “Hal: Hybrid assistive limb based on cybernics,” in *Robotics Research, Springer Tracts in Advanced Robotics* (M. Kaneko and Y. Nakamura, eds.), pp. 25–34, Springer, 2011.
- [23] S. H. Collins, M. B. Wiggin, and G. S. Sawicki, “Reducing the energy cost of human walking using an unpowered exoskeleton,” *Nature*, vol. 522, no. 7555, p. 212, 2015.
- [24] A. Milenković, C. Otto, and E. Jovanov, “Wireless sensor networks for personal health monitoring: Issues and an implementation,” *Computer communications*, vol. 29, no. 13, pp. 2521–2533, 2006.
- [25] A. B. Zoss, H. Kazerooni, and A. Chu, “Biomechanical design of the berkeley lower extremity exoskeleton (bleex),” *IEEE/ASME Transactions On Mechatronics*, vol. 11, no. 2, pp. 128–138, 2006.
- [26] M. P. De Looze, T. Bosch, F. Krause, K. S. Stadler, and L. W. OSullivan, “Exoskeletons for industrial application and their potential effects on physical work load,” *Ergonomics*, vol. 59, no. 5, pp. 671–681, 2016.
- [27] H. Kobayashi, D. Matsushita, Y. Ishida, and K. Kikuchi, “New robot technology concept applicable to human physical support -the concept and possibility of the muscle suit (wearable muscular support apparatus)-,” *J. of Robotics and Mechatronics*, vol. 14, no. 1, pp. 46–53, 2002.
- [28] K. Kong and D. Jeon, “Design and control of an exoskeleton for the elderly and patients,” *IEEE/ASME Transactions on mechatronics*, vol. 11, no. 4, pp. 428–432, 2006.
- [29] J. F. Veneman, R. Kruidhof, E. E. Hekman, R. Ekkelenkamp, E. H. Van Asseldonk, and H. Van Der Kooij, “Design and evaluation of the lopes exoskeleton robot for interactive gait rehabilitation,” *IEEE Transactions on Neural Systems and Rehabilitation Engineering*, vol. 15, no. 3, pp. 379–386, 2007.

-
- [30] C. N. Schabowsky, S. B. Godfrey, R. J. Holley, and P. S. Lum, “Development and pilot testing of hexorr: hand exoskeleton rehabilitation robot,” *Journal of neuroengineering and rehabilitation*, vol. 7, no. 1, p. 36, 2010.
- [31] “INNOPHYS CO. ,LTD..” <https://innophys.jp/product/>, 2017.
- [32] “Cyberdyne inc..” <https://www.cyberdyne.jp>, 2017.
- [33] “RB3D.” <https://www.rb3d.com/>, 2017.
- [34] “Standard performance test of wearable robots for lumbar support (in japanese), japanese industrial standards committee.” <https://www.jisc.go.jp/app/jis/general/GnrJISNumberNameSearchList?toGnrJISStandardDetailList>, 11 2019.
- [35] C. Nabeshima, K. Ayusawa, C. Hochberg, and E. Yoshida, “Standard performance test of wearable robots for lumbar support,” *IEEE Robotics and Automation Letters*, vol. 3, no. 3, pp. 2182–2189, 2018.
- [36] Y. Nakamura, K. Yamane, Y. Fujita, and I. Suzuki, “Somatosensory computation for man-machine interface from motion-capture data and musculoskeletal human model,” *IEEE Transactions on Robotics*, vol. 21, no. 1, pp. 58–66, 2005.
- [37] S.-H. Lee, E. Sifakis, and D. Terzopoulos, “Comprehensive biomechanical modeling and simulation of the upper body,” *ACM Transactions on Graphics (TOG)*, vol. 28, no. 4, p. 99, 2009.
- [38] “Open sim.” <https://opensim.stanford.edu>, 12 2019.
- [39] S. L. Delp, F. C. Anderson, A. S. Arnold, P. Loan, A. Habib, C. T. John, E. Guendelman, and D. G. Thelen, “Opensim: open-source software to create and analyze dynamic simulations of movement,” *IEEE transactions on biomedical engineering*, vol. 54, no. 11, pp. 1940–1950, 2007.
- [40] “Anybody technology.” <https://www.anybodytech.com>, 12 2019.

-
- [41] M. Damsgaard, J. Rasmussen, S. T. Christensen, E. Surma, and M. De Zee, “Analysis of musculoskeletal systems in the anybody modeling system,” *Simulation Modelling Practice and Theory*, vol. 14, no. 8, pp. 1100–1111, 2006.
- [42] C. Pizzolato, M. Reggiani, L. Modenese, and D. Lloyd, “Real-time inverse kinematics and inverse dynamics for lower limb applications using opensim,” *Computer methods in biomechanics and biomedical engineering*, vol. 20, no. 4, pp. 436–445, 2017.
- [43] J. B. Langholz, G. Westman, and M. Karlsteen, “Musculoskeletal modelling in sports-evaluation of different software tools with focus on swimming,” *Proceedia engineering*, vol. 147, pp. 281–287, 2016.
- [44] M. Mirakhorlo, M. R. Azghani, and S. Kahrizi, “Validation of a musculoskeletal model of lifting and its application for biomechanical evaluation of lifting techniques,” *Journal of research in health sciences*, vol. 14, no. 1, pp. 23–28, 2013.
- [45] P. Agarwal, M. S. Narayanan, L.-F. Lee, F. Mendel, and V. N. Krovi, “Simulation-based design of exoskeletons using musculoskeletal analysis,” in *ASME 2010 International Design Engineering Technical Conferences and Computers and Information in Engineering Conference*, pp. 1357–1364, American Society of Mechanical Engineers Digital Collection, 2010.
- [46] K. Cho, Y. Kim, D. Yi, M. Jung, and K. Lee, “Analysis and evaluation of a combined human-exoskeleton model under two different constraints condition,” *Proceedings of the International Summit on Human Simulation*, pp. 23–25, 2012.
- [47] P. Konrad, “The abc of emg: A practical introduction to kinesiological electromyography,” *version*, vol. 1, pp. 29–33, 2005.
- [48] H. Kobayashi, T. Aida, and T. Hashimoto, “Muscle suit development and factory application,” *Int. J. of Automation Technology*, vol. 3, no. 6, pp. 709–715, 2009.

-
- [49] T. Mattioli and M. Vendittelli, “Interaction force reconstruction for humanoid robots,” *IEEE Robotics and Automation Letters*, vol. 2, no. 1, pp. 282–289, 2017.
- [50] J. Vorndamme, M. Schappler, and S. Haddadin, “Collision detection, isolation and identification for humanoids,” in *Robotics and Automation (ICRA), 2017 IEEE International Conference on*, pp. 4754–4761, IEEE, 2017.
- [51] S. Faraji and A. J. Ijspeert, “Designing a virtual whole body tactile sensor suit for a simulated humanoid robot using inverse dynamics,” in *2016 IEEE/RSJ Int. Conf. on Intelligent Robots and Systems (IROS)*, pp. 5564–5571, 10 2016.
- [52] W. Khalil and E. Dombre, *Modeling, identification and control of robots*. London-U.K: Hermès Penton, 2002.
- [53] K. Ayusawa, G. Venture, and Y. Nakamura, “Identifiability and identification of inertial parameters using the underactuated base-link dynamics for legged multibody systems,” *Int. J. of Robotics Research*, vol. 33, no. 3, pp. 446–468, 2014.
- [54] K. Ayusawa, M. Morisawa, and E. Yoshida, “Motion retargeting for humanoid robots based on identification to preserve and reproduce human motion features,” in *Proc. 2015 IEEE/RSJ Int. Conf. on Intelligent Robots and Systems*, pp. 2774–2779, 2015.
- [55] O. Dahl and L. Nielsen, “Torque-limited path following by online trajectory time scaling,” *IEEE Transactions on Robotics and Automation*, vol. 6, no. 5, pp. 554–561, 1990.
- [56] H. Arai, K. Tanie, and N. Shiroma, “Time-scaling control of an underactuated manipulator,” *Journal of the Robotics Society of Japan*, vol. 16, no. 4, pp. 561–568, 1998.

-
- [57] K. Kaneko, F. Kanehiro, M. Morisawa, K. Akachi, G. Miyamori, A. Hayashi, and N. Kanehira, “Humanoid robot HRP-4 - humanoid robotics platform with lightweight and slim body,” in *Proc. 2011 IEEE/RSJ Int. Conf. on Intelligent Robots and Systems*, pp. 4400–4407, 2011.
- [58] Y. Nakamura and H. Hanafusa, “Inverse kinematic solutions with singularity robustness for robot manipulator control,” *ASME, Transactions, Journal of Dynamic Systems, Measurement, and Control*, vol. 108, pp. 163–171, 1986.
- [59] T. Ito, K. Ayusawa, E. Yoshida, and H. Kobayashi, “Human motion reproduction by torque-based humanoid tracking control for active assistive device evaluation,” in *2017 IEEE-RAS 17th International Conference on Humanoid Robotics (Humanoids)*, pp. 503–508, IEEE, 2017.
- [60] A. De Luca and R. Mattone, “Actuator failure detection and isolation using generalized momenta,” in *2003 IEEE International Conference on Robotics and Automation (Cat. No. 03CH37422)*, vol. 1, pp. 634–639, IEEE, 2003.
- [61] A. De Luca and R. Mattone, “Sensorless robot collision detection and hybrid force/motion control,” in *Proceedings of the 2005 IEEE international conference on robotics and automation*, pp. 999–1004, IEEE, 2005.
- [62] A. J. Ijspeert, J. Nakanishi, H. Hoffmann, P. Pastor, and S. Schaal, “Dynamical movement primitives: learning attractor models for motor behaviors,” *Neural computation*, vol. 25, no. 2, pp. 328–373, 2013.
- [63] M. Okada and M. Watanabe, “Controller decomposition and combination design of body/motion elements based on orbit attractor,” in *2009 IEEE International Conference on Robotics and Automation*, pp. 1364–1369, IEEE, 2009.
- [64] R. Dumas, L. Cheze, and J.-P. Verriest, “Adjustments to mcconville et al. and young et al. body segment inertial parameters,” *Journal of biomechanics*, vol. 40, no. 3, pp. 543–553, 2007.

List of Publications

Journals

- [1] Takahiro Ito, Ko Ayusawa, Eiichi Yoshida, and Hiroshi Kobayashi, "Evaluation of Active Wearable Assistive Devices with Human Posture Reproduction using a Humanoid Robot," *Advanced Robotics*, vol. 32, no. 12, pp. 635-645, 2018.
- [2] Takahiro Ito, Ko Ayusawa, Eiichi Yoshida, and Hiroshi Kobayashi, "Simultaneous Control Framework for Humanoid Tracking Human Movement with Interacting Wearable Assistive Device," *IEEE Robotics and Automation Letters*, (to appear).
- [3] Manuel Giuseppe Catalano, Irene Frizza, Cecilia Morandi, Giorgio Grioli, Ko Ayusawa, Takahiro Ito, Gentiane Venture, "HRP-4 walks on Soft Feet," *IEEE Robotics and Automation Letters*, (to appear).

Reviewed Conference Papers

- [1] Takahiro Ito, Ko Ayusawa, Eiichi Yoshida, and Abderrahmane Kheddar, "Experimental study for controller-friendly contact estimation for humanoid robot," in *15th IEEE International Conference on Advanced Robotics and its Social Impacts (ARSO2019)*, pp. 28-33, 2019.

- [2] Takahiro Ito, Ko Ayusawa, Eiichi Yoshida, and Hiroshi Kobayashi, "Human motion reproduction by torque-based humanoid tracking control for active assistive device evaluation," in 2017 IEEE-RAS 17th International Conference on HumanoidRobotics (Humanoids), pp. 503-508, IEEE, 2017.
- [3] Takahiro Ito, Ko Ayusawa, Eiichi Yoshida, and Hiroshi Kobayashi, "Stationary Torque Replacement for Evaluation of Active Assistive Devices using Humanoid," in Proc. 2016IEEE-RAS Int. Conf. on Humanoid Robots, pp. 739-744, 11 2016.

Oral Presentations (in Japanese)

- [1] Takahiro Ito, Eiichi Yoshida, Ko Ayusawa and Hiroshi Kobayashi, "Evaluation of Active Assistive Devices by Human Motion Reproduction on Humanoid Robot," in Proc. of the 34th Annual Conference of the Robotics Society of Japan, 2016.
- [2] Takahiro Ito, Ko Ayusawa, Eiichi Yoshida, and Hiroshi Kobayashi, "Human Motion Reproduction by Humanoid Tracking Control for Active Assistive Device Evaluation," in Proc. of the 2017 JSME Conference on Robotics and Mechatronics, 1A1-O10, 2017.

